Ore Geology Reviews 104 (2019) 522–539

Contents lists available at ScienceDirect

Ore Geology Reviews

journal homepage: www.elsevier.com/locate/oregeorev

A new hypothesis on parameters controlling the formation and size of porphyry copper deposits: Implications on thermal gradient of subducted oceanic slab, depth of dehydration and partial melting along the Kerman copper belt in Iran

Mohammad Hassan Karimpour[a,*], Martiya Sadeghi[b]

[a] Research Centre for Ore Deposits of Eastern Iran, Faculty of Science, Ferdowsi University of Mashhad, Mashhad, Iran
[b] Mineral Resource Department, Geological Survey of Sweden, Uppsala, Sweden

ARTICLE INFO

Keywords:
Porphyry copper formation
Iran
Subduction zone geodynamics
Thermal gradient
Dehydration and partial melting

ABSTRACT

Porphyry copper deposits in the Tethyan metallogenic belt broadly occur in early Mesozoic, late Mesozoic, Paleogene, and Neogene within a wide range of tectonic setting. These deposits in Iran often occur within the Cenozoic Urumieh-Dokhtar Magmatic Arc (UDMA), mostly in the Kerman porphyry copper belt (KPCB) located in the southeast of this arc. These deposits along the UDMA are mainly associated with the granitoids of Miocene age (18.82–9.20 Ma). In this research, geochemical characteristics, Pb and Sr isotopes, tectonic environment, oxidizing conditions and source of magmas for the most important porphyry copper deposits of the UDMA have been compared and discussed. On the basis of trace element discrimination diagrams, the Kerman belt granitoids formed in a volcanic arc-type setting, whereas the Jebal Barez granitoids seem to have formed in a different tectonic setting. The Eu/Eu^{*} of granitoids from the Kerman belt are greater than 1.2, representing the oxidizing conditions for the crystallization of the granitoid magma, whereas Jebal Barez granitoids were formed under reducing conditions. The Sr/Y ratio for Kerman granitoids is greater than 60, indicating adakitic affinities and (La/Yb)n for these granitoid rocks is between 17 and 35, suggesting that their parental magma was generated from a deep garnet-bearing source. Based on $(^{87}Sr/^{86}Sr)i$ values for Kerman belt granitoids of 0.704–0.705, it is suggested that parental magmas originated from a subducted oceanic slab. In the Sarcheshmeh porphyry copper deposit, the thermal gradient of the oceanic slab at depth was less than 9 °C/Km (warm-cold slab). The oceanic slab was highly hydrated and more than 80% of the water within the oceanic slab was released in the deep zone of the sub-arc region at a depth of 110–130 Km. Under saturated conditions, the oceanic slab partially melted (20–25%). A large volume of magma and magmatic water formed Sarcheshmeh as a giant porphyry copper deposit. In the Iju deposit, a small porphyry copper deposit, the oceanic slab was slightly hydrated and minor water was released at the depth of 110–130 Km. A small volume of magma was formed due to water under-saturated melting conditions. Finally, a *new hypothesis* is introduced regarding the roles of down-dip thermal gradient of the oceanic slab, water content, depth of dehydration and degree of partial melting of oceanic slab which are important controls on the formation and size of the porphyry copper deposits within continental volcanic arcs.

1. Introduction

Porphyry copper deposits mostly include the world's largest copper deposits in the global economy. About 75% of world copper, 50% of molybdenum and 20% of gold are produced from porphyry copper deposits (Sillitoe, 2010) with an average ore grade of 0.45–1.5% Cu, 0.007–0.04% Mo and up to 1.5 ppm Au. Ore reserves for most porphyry copper deposits are typically between 20 and 10,000 million tons (Sillitoe, 2010; Kesler et al., 2002). World copper metal production in 2017 was 19,700,000 tons (Mineral Commodity Summaries, 2018).

Porphyry copper systems are defined as large volumes of hydrothermally altered rock centered on porphyry Cu stocks (Sillitoe, 2010). These systems are products of shallow crustal emplacement of hydrous arc magmas and some collisional and post-subduction magmas

* Corresponding author at: Research Centre for Ore Deposits of Eastern Iran, Faculty of Science, Ferdowsi University of Mashhad, P.O. Box No. 91775-1436, Mashhad, Iran.
E-mail address: karimpur@um.ac.ir (M.H. Karimpour).

https://doi.org/10.1016/j.oregeorev.2018.11.022
Received 9 June 2018; Received in revised form 26 October 2018; Accepted 20 November 2018
Available online 22 November 2018
0169-1368/

(Richards, 2018). The most fertile sources for syn-and post-collisional porphyry deposits appear to be related to subduction-modified lithosphere, because these hydrated lithologies melt at relatively low temperatures during later tectono-magmatic events and retain the oxidized and relatively metalliferous character of the original arc magmatism (Richards, 2015). Porphyry copper deposits are commonly associated with intermediate composition arc-related igneous rocks with high Sr/Y and La/Yb ratios (Richards, 2011). Igneous rocks having ratios of Sr/Y > 25 and Y < 10 ppm are considered as adakitic type. A high ratio of Sr/Y is an indicator that magma was generated at greater depth within the subduction zone. To discriminate between the sources of ore-bearing magmas and barren magmas and, the relationship between fertilizing porphyry copper and the deep source of magma, a ratio of Sr/Y > 25 of igneous rocks is proposed by Wan et al. (2018) and Deng et al. (2018).

Porphyry Cu systems were generated worldwide since the Archean, although Mesozoic and Cenozoic examples are most frequently preserved (Singer et al., 2008), probably because of limited erosion in the younger arc terranes (e.g. Seedorff et al., 2005; Kesler and Wilkinson, 2006; Wilkinson and Kesler, 2009). Over 50 percent of the giant porphyry copper deposits are located in north and central Chile, southwest Arizona, and northern Mexico. There are also other giant deposits in Montana, Utah, Panama, Peru, Argentina, Mongolia and Iran. Comprehensive tectonic environments, thickened continental crust, active uplift and erosion were associated with the formation of many of these deposits. (Cooke et al., 2005).

Several tectonic models for porphyry Cu mineralization within collisional orogenic belts were proposed by various authors and summarized by Pirajno (2009). However, porphyry copper deposits can be directly related to subduction (e.g. occurrences of the giant Saindak and Reko Diq porphyry Cu-Au deposits in western Pakistan) or copper and gold deposits related to post-subduction tectonic setting or collisional processes (e.g., Roşia Montană in Romania, Kisladag in Turkey, and Sari Gunay in Iran. Skouries deposit in Greece, Sungun, Meiduk, and Sar Cheshmeh in Iran and Qulong in southern Tibet are other examples of porphyry deposits related to subduction tectonic setting.

Porphyry formation in the Tethyan orogen is broadly divided into four main episodes: early Mesozoic (Triassic-Jurassic), late Mesozoic (Cretaceous), Paleogene, and Neogene (Richards, 2015). The wide range of tectonic settings represented along the Neotethyan orogenic belt thus provides a good opportunity to study porphyry ore formation in response to different geodynamic processes. Richards (2015) reviewed and summarized the tectonic, magmatic and metallogenic history of the Tethyan orogen from the Carpathians to Indochina which can be one of the fundamentals for understanding the formation of porphyry copper deposits in different tectonic settings and the role of magmatic evolution.

All known large porphyry copper deposits in Iran occurred within the Cenozoic Urumieh-Dokhtar Magmatic Arc (UDMA) (McInnes et al., 2003, Shafiei et al., 2008, 2009; Hou et al., 2011; Richards et al., 2012). They are mostly located in the southeastern arc segment of the UDMA that is called the Kerman Cenozoic magmatic arc (KCMA; Shafiei et al., 2009a,b). This arc is associated with calc-alkaline stocks and was interpreted by Dewey et al. (1973) as an Andean-type Cordilleran arc system within the collisional Alpine-Himalayan orogenic belt. Transition from normal calc-alkaline arc magmatism in the Eocene-Oligocene (Jebal-Barez-type) to adakite-like calc-alkaline magmatism (Kuh Panj-type) in the mid-late Miocene-Pliocene reflects the onset of collision between the Afro-Arabian and Eurasian plates in the Kerman Cenozoic arc segment (Asadi et al., 2014). Cenozoic magmatism in the Urumieh-Dokhtar belt has been the focus of many exploration companies as it is related to several large porphyry Cu deposits, mainly of Miocene age. In addition, several researchers have worked on the magmatism, tectonic setting and genesis of porphyry copper systems belonging to this belt (Ahmadian et al., 2009; Alaminia et al., 2013; Arjmandzadeh and Santos, 2014; Hou et al., 2011; McInnes et al., 2003; McInnes et al., 2005; Razique et al., 2007; Richards et al., 2012; Shafiei et al., 2009a,b; Shafiei and Shahabpour, 2008; Taghipour, 2007; Taghipour et al., 2008; Zarasvandi et al., 2005; Zarasvandi et al., 2015). In general, it is agreed that Neotethyan subduction started from Triassic in Iran. (Kazemi et al., 2018 and reference therein) but this subduction was continued until the collision of Arabia and Eurasia in the Late Cretaceous to Oligocene-Miocene as the closure age of the Neotethyan ocean (Kazemi et al., 2018).

A number of key factors contributed to the potential for an arc magmatic system to generate an economic porphyry copper-molybdenum-gold deposit. Of these, the following factors are most important such as; high magma flux (Richards, 2018), high magmatic water, sulfur and chlorine content (Cooke et al., 2005; Sillitoe, 2010; Richards, 2018), magma oxidation above normal mantle values (Richards, 2018), rate and angle of subduction, the oxidation of the slab, mantle wedge and upper plate lithosphere, and the state of stress in the crust. Although the ore-forming mechanism and important key factors contributing to the formation of giant porphyry copper is still debated. The aim of this paper is to present the age and petrogenesis of granitoids within the Kerman Porphyry Copper Belt (KPCB) as well as the granitoids within the Jebal Barez belt, and also introduce a *new hypothesis* regarding the role of the thermal gradient, water content and depth of dehydration of subducted oceanic slab as key factors which control the size and ore grades in porphyry copper systems within continental volcanic arcs and specifically along Kerman magmatic arc porphyry system.

2. Geology of porphyry copper deposits in Iran

Based on geology and tectonic setting, Iran has great potential for exploration of different types of mineral commodities. All Iranian porphyry copper deposits along the UDMA (mainly formed in Miocene time) and in Eastern Iran (formed in Eocene-Oligocene) are post-collisional type (Aghazadeh et al., 2015; Golestani et al., 2018; Shafiei, 2010; Karimpour et al., 2012). The porphyry copper deposits in Iran are clustered in several metallogenic zones or belts such as Kerman, Arasbaran, Saveh-Yazd, as well as Eastern Iran (Fig. 1). The locations of porphyry copper belts and deposits are shown in Fig. 1. These deposits are mostly associated with Tertiary granitoid rocks.

Eastern Iran Porphyry copper deposits: Porphyry copper deposits in Eastern Iran are mostly located within the Lut block formed during Late Eocene time, from 39 to 28 Ma (Karimpour et al., 2012). Major rocks within the Lut block are Tertiary sub-volcanics (monzonite, quartz monzonite, diorite and quartz diorite) and volcanic rocks (mainly andesite, dacite and minor rhyolite). Maherabad and Shadan are major porphyry copper-gold deposits in this area (Malekzadeh Shafaroudi et al., 2015, 2010) (Table 1). Gazu is the only porphyry copper system which formed in the Late Cretaceous (68 Ma) in this area (Mahdavi et al., 2016). This area also has great exploration potential for small scale porphyry copper and gold deposits (Karimpour et al., 2012) such as: Mehrabad and Shadan porphyry copper gold (Malekzadeh Shafaroudi et al., 2015, 2010), Tannurjeh (Hossieni et al., 2018), Firouzeh Neyshabour (Ghiasvand et al., 2018), Halak Abad (Ghourchi et al., 2014), Baharieh (Almasi et al., 2017), Chah Shaljami (Arjmandzadeh et al., 2011a), Mahour (Miri Beydokhti et al., 2015), Cheshmeh Sabz (Javidi Moghadam et al., in press), Dehsalm (Arjmandzadeh et al., 2011b), and Kuh Shah (Abdi et al., 2013).

Arasbaran Porphyry copper belt: The Arasbaran belt, located in northwestern Iran, has a great exposure of Tertiary igneous rocks, both volcanic and sub-volcanic rocks. Sungun and Masjed Daghi are the most important porphyry deposits along this belt (Fig. 2) which are active at present (Table 2). Sungun and Masjed Daghi porphyry copper deposits were formed in the Early Miocene (21 & 20.5 Ma, Table 2, Aghazadeh et al., 2015). This part of Iran has great exploration potential for porphyry copper, molybdenum and various types of epithermal gold deposits.

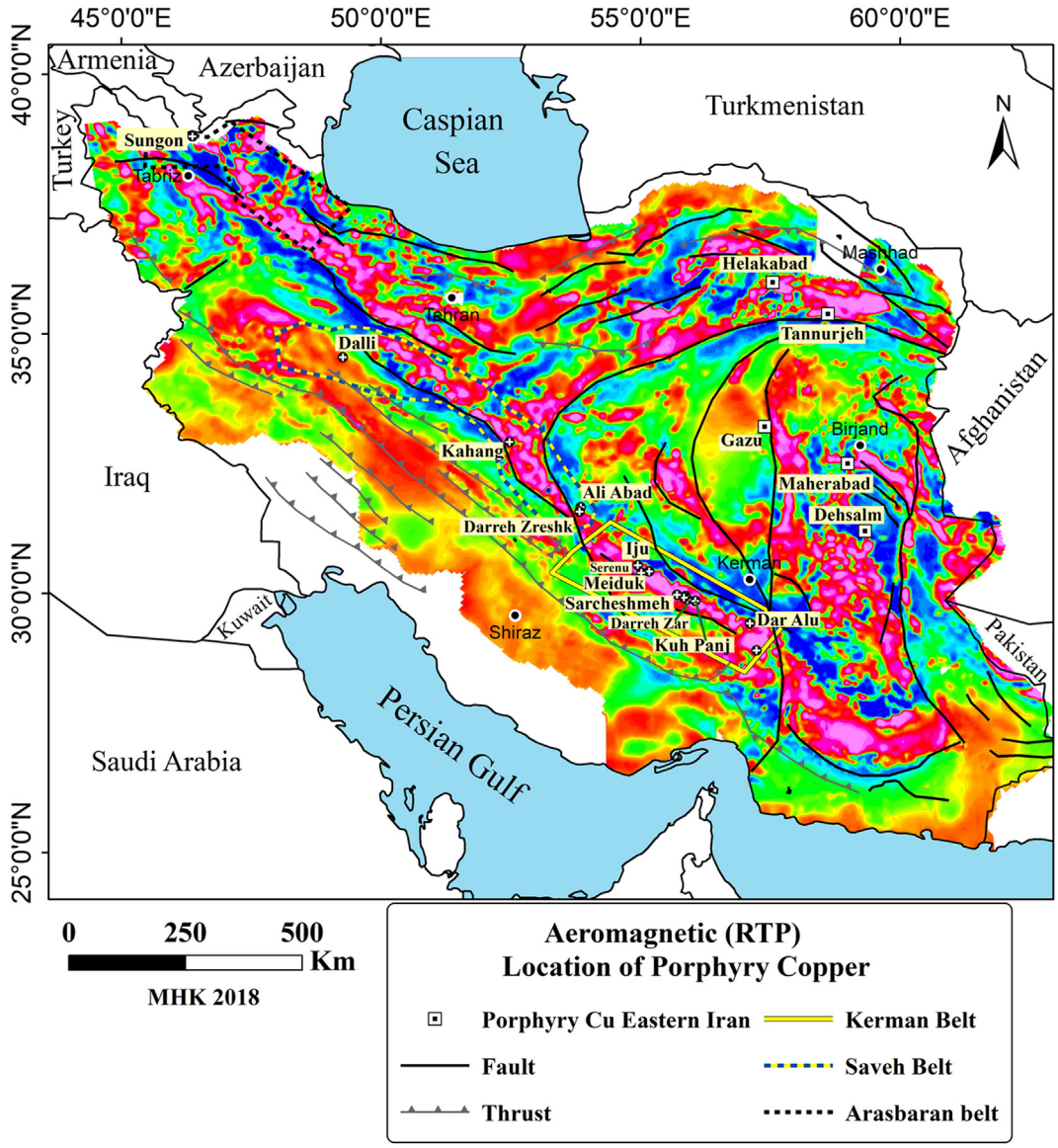

Fig. 1. Location of major porphyry copper belts and deposits.

Saveh-Yazd Porphyry copper belt: The Saveh-Yazd porphyry copper belt is located in the middle portion of the UDMA (Fig. 1). Dalli, Darreh Zereshk, Kahang, and Ali Abad porphyry Cu (Au, Mo) deposits were also recently discovered along this belt (Fig. 1). These deposits were formed during the Early to Middle Miocene (Table 3). The ore reserve and ore grades of these deposits are listed in Table 3.

Kerman Porphyry copper belt: (Fig. 2). The UDMA extends about 2000 Km in a NW-SE direction in Iran. The KPCB is situated in the southeast of the UDMA and extends about 350 Km (Fig. 2). Magmatic activities along the KPCB are Tertiary granitoids and volcanic rocks (Paleocene-Eocene-Oligocene-Miocene) (Sarjoughian and Kananian, 2017; Omrani et al., 2008) associated with the subducting Neo-Tethys oceanic slab (Sarjoughian and Kananian, 2017; Omrani et al., 2008; Agard et al., 2005, 2011; Alavi, 2004; Alavi, 2007; Alavi and Mahdavi, 1994). Granitoids were emplaced during several episodes from the Paleocene to Miocene. Their location and timing were different along this belt (Honarmand et al., 2013). The age and the volume of magmatic activities along this belt are different (Chiu et al., 2013; Azizi et al., 2011).

The KPCB is the most important metallogenic zone in Iran and several porphyry copper deposits occurred along this belt (Fig. 3). The porphyry copper deposits along this belt are mostly associated with granitoids which have been formed during a specific period (mostly Oligo-Miocene) and location (Aghazadeh et al., 2015; Golestani et al., 2018; Shafiei, 2010). Sarcheshmeh is the largest porphyry copper deposit in Iran along this belt. Miocene age sub-volcanic granitoids

Table 1
Porphyry copper gold deposits in Eastern Iran.

	Deposit	Age (Ma)	Coordinates	References
Lut Block	Maherabad	**39**	32°30′N, 58°59′E	Malekzadeh Shafaroudi et al. (2015)
Lut Block	Shadan	**39**	32°22′N, 58°56′E	Malekzadeh Shafaroudi et al. (2015)
Tabas Block	Gazu	**68**	33°12′N, 57°23′E	Mahdavi et al. (2016)

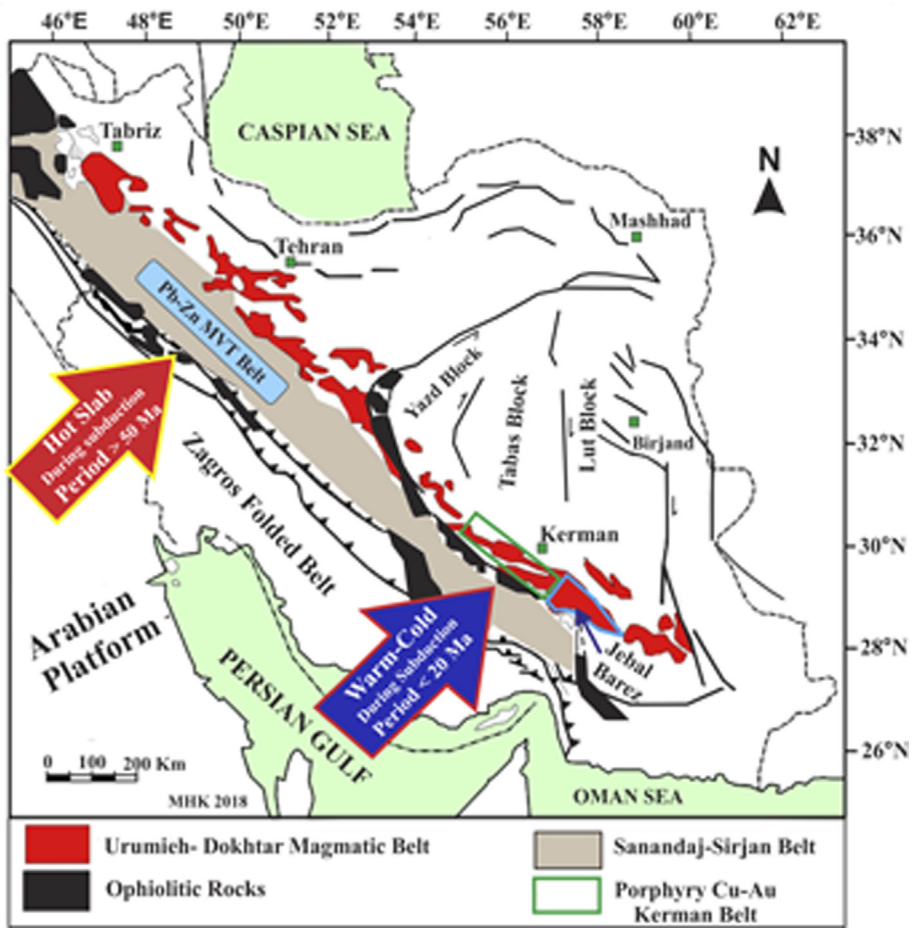

Fig. 2. Map showing the location of the Kerman porphyry copper belt.

intruded the older Tertiary volcanic rocks. The composition of granitoid rocks at Sarcheshmeh and Meiduk range from monzonite to granodiorite and diorite, but younger deposits such as Iju and Serenu are mainly hosted by diorite and quartz diorite.

3. Grade, tonnage, and age

Sarcheshmeh deposit (Fig. 3) with 1200 Mt ore reserve with average grades of 0.85% Cu, 0.03% Mo and 0.06 ppm Au is one of the world largest porphyry copper deposits (Table 4). Meiduk deposit (Fig. 3) with 176 Mt of ore reserves and Cu grade at 0.61% is the second largest porphyry deposit within the Kerman belt (Table 4). Ore reserves and grades of the most important porphyry copper deposits along the KPCB are listed in Table 4.

As shown in Fig. 4 and Table 3, the ages of most of the porphyry copper deposits along the UDMA are from 17.85 to 9 Ma. Porphyry copper deposits along Kerman belt mostly formed from 15.5 to 9 Ma. Sarcheshmeh and Meiduk formed during Miocene (13.6–12.5 Ma) while there are small size porphyry copper deposits which are 1 or 2 million years older than 13.6 Ma (Fig. 3) (i.e.; Sar Kuh, Darreh Zar, and Now Chun) (Table 4). There are also small porphyry copper deposits around Meiduk such as Chah Firouzeh and Chah Messi (Fig. 3). Within KPCB there are smaller porphyry copper deposits such as Iju, Sereno and Abdar, which are mostly younger than 10 Ma (e.g., Table 4, Fig. 3).

Fig. 4 shows a comparison between the ages of porphyry copper deposits in Iran. Gazu is the oldest porphyry copper deposit located in Eastern Iran at 68 Ma and in general the Eastern Iran porphyry copper deposits are older compared to the KPCB (Fig. 4). The gold content of porphyry copper deposits in Eastern Iran is higher in comparison with other deposits in Iran (Malekzadeh Shafaroudi et al., 2015).

To determine the size of alteration zones within the porphyry copper deposits, mineral mapping with ASTER satellite data (The Advanced Spaceborne Thermal Emission and Reflection Radiometer) has been applied. Spectral Angle Mapper (SAM) method was used for mineral mapping. Distribution of end-members are mapped by using the SAM in VNIR and SWIR of ASTER bands (Karimpour et al., 2014; Honarmand, 2016; Rowan et al., 2003). Since propylitic and sericitic alteration zones are important, mineral mapping was done only for chlorite, epidote and muscovite. Propylitic (chlorite & epidote) and sericitic alteration zones are shown in Figs. 5 and 6. The sericite, chlorite and epidote alteration zones around Sarcheshmeh porphyry copper mine are very large (> 5 Km wide, Fig. 5). The size of alteration

Table 2
Ore reserve and ore grade of Sungun and Masjed Daghi mines.

	Ore reserve MT	Cu%	Mo%	Au (ppm)	Age	Coordination	
Sungun	740	0.66	0.024	–	21	38°43′N, 46°42′E	Aghazadeh et al. (2015)
Masjed Daghi	240	0.34	–	2	20.5	39°8′N, 46°8′E	Aghazadeh et al. (2015)

Table 3
Ore reserve and ore grade of porphyry copper along Saveh-Yazd belt. (USGS, Mineral Resources On-Line Spatial Data, Komeili et al., 2017).

	Ore reserve MT	Cu%	Mo%	Au (ppm)	**Age Ma**	Coordinates	References
Kahang	40	0.53	0.02	–	**15.1**	32°55′N, 52°28′E	Ayati et al. (2013)
Darreh Zereshk	23	0.9	0.004	–	**16.5**	31°33′N, 53°50′E	Zarasvandi et al. (2005)
Ali Abad	40	0.73	0.0059	–	**16.5**	31°38′N, 53°50′E	Zarasvandi et al. (2005)
Dalli	8	0.5	–	0.75	**21**	34°16′N, 50°19′E	Ayati et al. (2013)

around Darreh Zar is about 1.5 km, around Meiduk deposits is around 2.5 km and around Iju deposits is less than 1 km (Fig. 5).

4. Geochemistry of trace elements and isotopes

There are two main plutonic belts within the Kerman Cenozoic arc segment; the KPCB and the Jebal-Barez Belt (Fig. 2). The age of granitoid rocks within the KPCB is between 17.5 and 9 Ma and the Jebal-Barez granitoids are older than 20 Ma. The composition of granitoids ranges between quartz monzonite, monzonite, granodiorite, diorite and quartz diorite in both belts. The tectonic setting and the source magmas were different in both belts.

Trace element discrimination diagrams (Pearce et al., 1984) show that the granitoid rocks from KPCB plotted in the field of volcanic arc tectonic settings, but the Jebal-Barez granitoids plotted in the field of intraplate tectonic settings (Fig. 7). This is very important to note that these two belts have totally different tectonic settings. Asadi et al. (2014) compared these two belts, discriminating between productive and barren porphyry copper deposits. Since porphyry copper deposits are only associated with *volcanic arc granitoid* rocks such as KPCB, it may lead to a wrong interpretation when *volcanic arc granitoids are* compared with granitoid rocks formed within another tectonic setting. Porphyry copper deposits are not associated with granitoid rocks formed within an intraplate tectonic setting.

To find the depth of magma generation and also the conditions of melting, REE geochemical data from Kerman porphyry copper granitoid rocks and Jebal-Barez belt are plotted in the (La/Yb)n versus Eu/Eu* diagram (Fig. 8). This diagram shows that the granitoid rocks from these two belts have formed in two different reducing and oxidizing conditions (Fig. 8). The ratio of Eu/Eu* is useful for finding the condition of magma generation (Fig. 8). The ratio of Eu/Eu* is less than one when the partial melting is under reducing conditions. If the ratio of Eu/Eu* is greater than one, it means that the magma was formed under oxidizing conditions (Fig. 8). The granitoid rocks in KPCB were formed under oxidizing conditions, whereas Jebal-Barez granitoids were formed under reducing conditions (Fig. 8).

The distribution coefficient of elements between magma and the source rock controls the ratio of (La/Yb)n. The distribution coefficient of La and Yb is quite different in some minerals such as garnet. The distribution coefficient of La in garnet is less than 0.01 and Yb is higher than 10. It means that a rock consisting of garnet during partial melting will produce a magma with a high concentration of La and a low concentration of Yb; therefore the ratio of (La/Yb)n will be high. The ratio of (La/Yb)n of granitoid rocks from KPCB is between 20 and 39 while the ratio of (La/Yb)n for granitoids rocks of the Jebal-Barez is less than 6 (Fig. 8). Granitoid rocks from KPCB were generated from a deep source where garnet was present, while the ratio of (La/Yb)n of the Jebal-Barez granitoid rocks is less than 6. Therefore, the magma was generated from a shallower depth (Fig. 8).

A spider diagram for the REE shows two distinct patterns for granitoid rocks of KPCB and Jebal-Barez (Fig. 9). LREE show strong enrichment and HREE are depleted in the granitoids of the KPCB (Fig. 9). This pattern also supports the plot in Fig. 8. Based on the patterns of the REE from granitoid rocks of KPCB and Jebal-Barez, the latest results do not show an enrichment in the LREE and depletion in the HREE (Fig. 9). This plot also supports that the magma source for the Jebal-Barez granitoid rocks was generated from a much shallower depth.

A plot of Y versus Sr/Y is used to discriminate the adakite-type and other granitoids. Granitoid rocks from KPCB are plotted in the field of

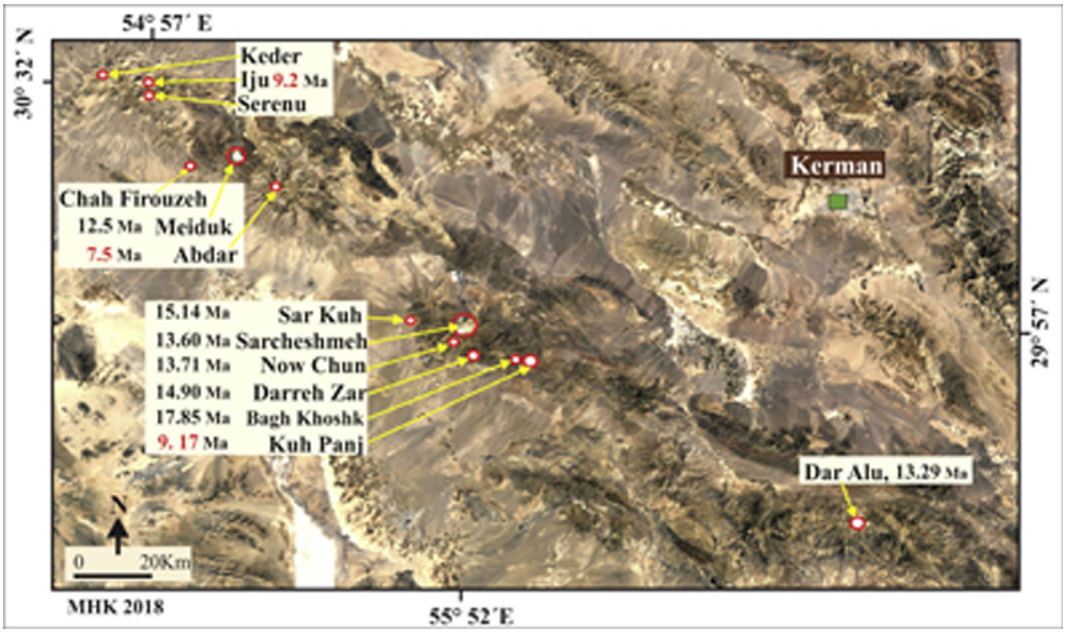

Fig. 3. Location of porphyry copper deposits within the Kerman belt.

Table 4
Ore reserve, grade, age and location of porphyry copper deposits along the KPCB.

Deposit	Reserve MT	Cu%	Mo%	Au ppm	Age Ma	Geographic coordinates	References
Iju	74	0.31	–	–	9.2	30°33′N, 54°57′E	Golestani et al. (2018)
Meiduk	176	0.61	0.007	0.05	12.5	30°20′N, 55°10′E	Aghazadeh et al. (2015)
Dar Alu	240	0.36	0.007	0.031	12.96	29°25′N, 57°06′E	Aghazadeh et al. (2015)
Sarcheshmeh	1200	0.85	0.03	0.06	13.6	29°56′N, 55°52′E	McInnes et al. (2003)
Now Chun	80	0.32	–	–	13.71	29°55′N, 55°51′E	Aghazadeh et al. (2015)
Darreh Zar	283	0.38	0.018	0.036	14.9	29°51′N, 55°53′E	Aghazadeh et al. (2015)
Sar Kuh	16	0.46	0.003	0.038	15.14	29°55′N, 57°46′E	Mirnejad et al. (2013)
Bagh Khoshk	24	0.27	–	–	17.85	29°49′N, 55°59′E	Aghazadeh et al. (2015)

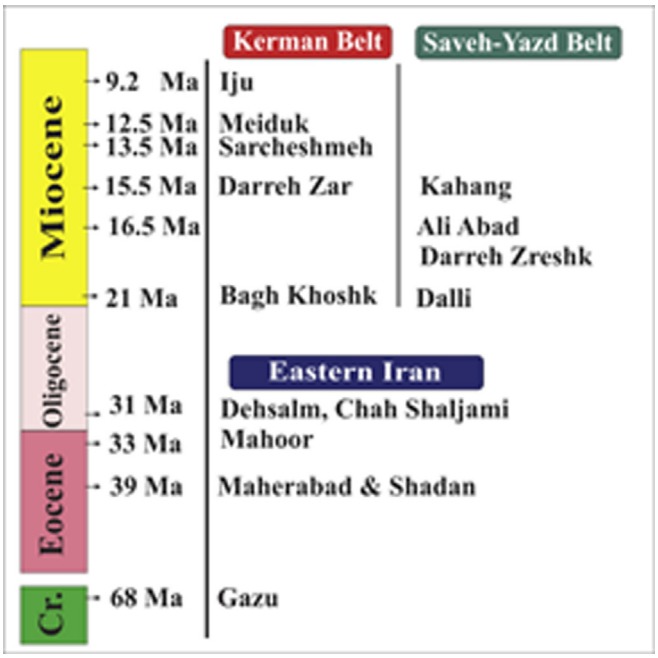

Fig. 4. Age of porphyry copper deposits in Iran.

adakite, while the Jebal-Barez granitoids are plotted in the field of low Sr and high Y (Fig. 10). This plot also proves that granitoid rocks from these two belts are totally different in tectonic setting and the origin.

Sr-isotope data of KPCB and Jebal-Barez granitoid rocks are reported in Table 5 and plotted in Fig. 11. The initial $(^{87}Sr/^{86}Sr)i$ of granitoid rocks from Jebal-Barez is greater than 0.7070. This indicates that the magma originated within the continental crust (Fig. 11). A low ratio of (La/Yb)n also indicates that the source of magma was from a shallower depth (Fig. 11).

The initial $(^{87}Sr/^{86}Sr)i$ of granitoid rocks from Kerman porphyry belt is less than 0.07047 (Table 5). The ratio of (La/Yb)n is high (20–39), therefore magma was generated from a very deep source (Fig. 11). On the basis of the both Sr-isotopes and (La/Yb)n it is concluded that the magma for ore-bearing granitoids of KPCB originated from subducted oceanic slab at depth.

The major differences between granitoid rocks of the KPCB and the Jebal Barez are as follows:

1. Based on the trace element discrimination diagrams (Pearce et al., 1984), the tectonic setting of the granitoid rocks of the KPCB was associated with a volcanic arc, whereas the Jebal-Barez granitoids were formed within an intraplate setting.
2. Based on initial Sr-isotopes, the magma of the KPCB granitoids originated from partial melting of an oceanic slab during the process of subduction, whereas magma of the granitoids at Jebal-Barez

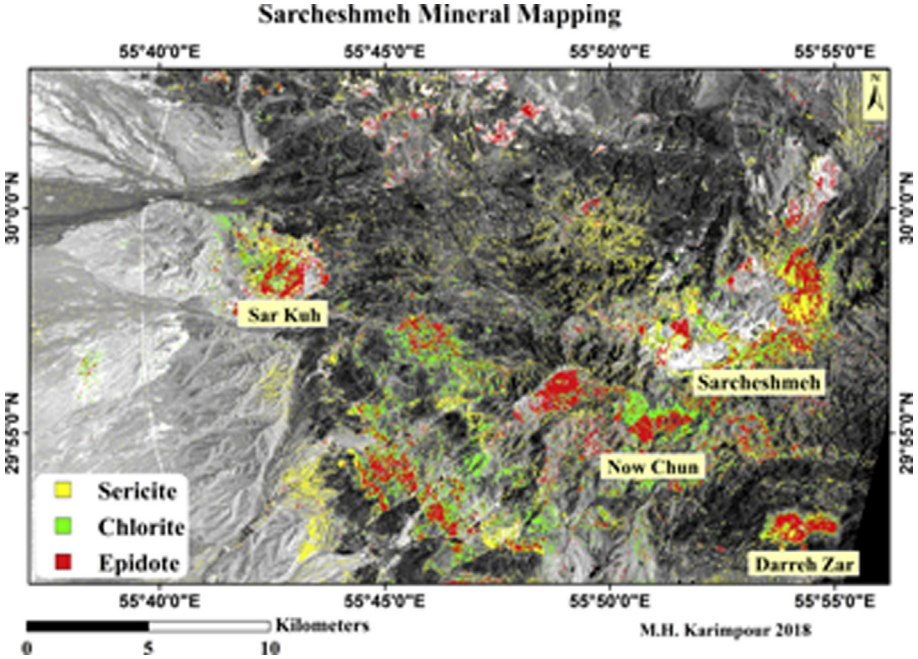

Fig. 5. Spectral Angle Mapper (SAM) method, ASTER mineral mapping of Sarcheshmeh and Kuh Panj porphyry copper deposits. The sericite, chlorite and epidote alteration zones around Sarcheshmeh porphyry copper mine are very large (> 5 Km wide).

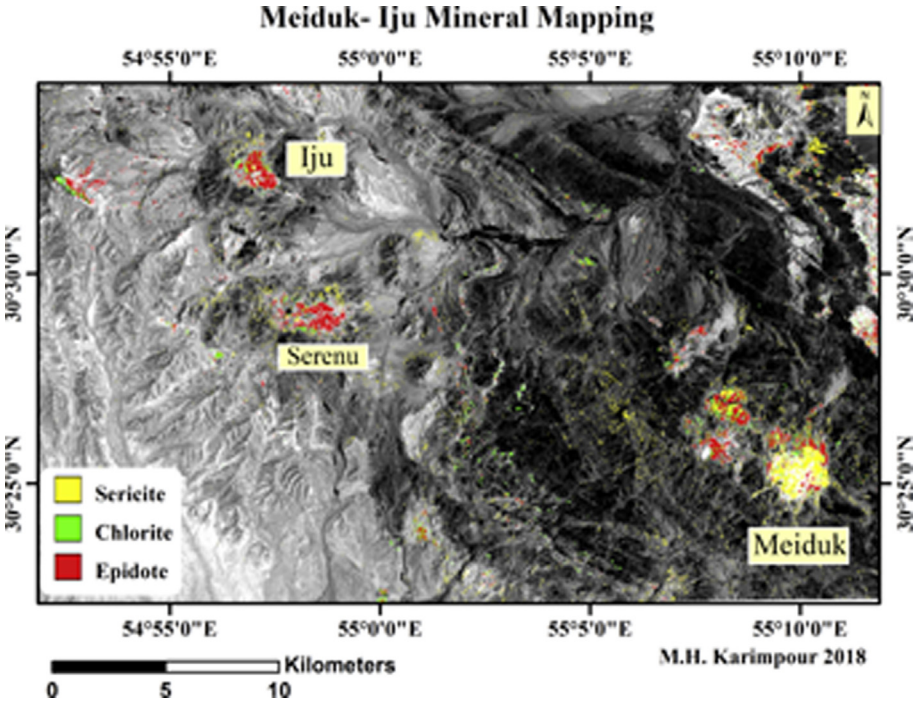

Fig. 6. ASTER mineral mapping of Meiduk and Iju porphyry copper deposits. The sericite, chlorite and epidote alteration zones around Meiduk porphyry copper mine is less than 2 Km wide and around Iju porphyry copper deposit is very small.

originated from the continental crust.

3. High ratio of (La/Yb)n Kerman granitoid rocks indicates the magma originated from a very deep source, while Jebal-Barez granitoids originated at shallower depth.
4. Granitoid rocks of KPCB have a ratio of $Eu/Eu^{*} > 1$ which means the magma formed under oxidizing conditions. Whereas the granitoid rocks from Jebal Barez granitoids have a ratio of $Eu/Eu^{*} < 1$ suggesting the magma was generated under reducing conditions.
5. Granitoid rocks of KPCB have a high ratio of Sr/Y, therefore they are adakitic, while the Jebal-Barez granitoids have low ratio Sr/Y and cannot be adakitic.

5. Hydration and dehydration of oceanic slab

In the following section, features such as the ***deep thermal gradient of the oceanic slab***, water content, depth of dehydration and degree of partial melting of oceanic slab which are very important for the formation of KPCB; will be explained.

5.1. Hydration of oceanic slab and water transport

Water plays an important role in subduction zones. Water within oceanic lithosphere is present as H_2O, OH^- and H. The total amount of water which is subducted by the oceanic lithosphere per year (global) is about 1.83×10^{15} g/yr (Jarrard, 2003).

Different sections of oceanic lithosphere contain different amounts of water. According to some researches (e.g. Rüpke et al., 2004; van Keken et al., 2011; Hacker, 2008), oceanic sediments contain 5–7% water, altered basalts and diabase contain 30–37% water, altered peridotites within the lower oceanic crust contain 25–29%, and the upper portion of altered mantle peridotites has 28–33% water. Serpentine minerals (antigorite, chrysotile, lizardite) carry most of the water and are the dominant hydrous minerals of oceanic lithosphere.

Serpentine, chlorite, and other hydrated minerals can form due to alteration in the following areas (Alt et al., 2007; Bach et al., 2004; Bonatti et al., 1984; Boschi et al., 2006; Delacour et al., 2008; Scambelluri et al., 2004; Vils et al., 2011). Significant amount of water contains carbon, sulfur, chlorine, boron, and arsenic will be migrated to

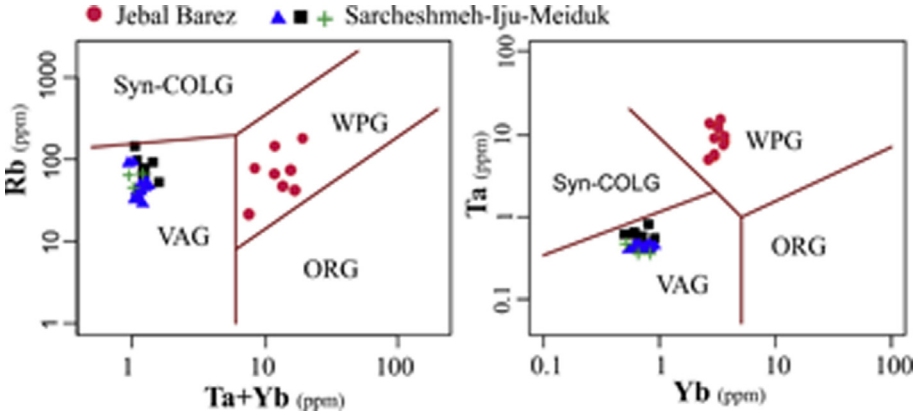

Fig. 7. Trace elements discrimination diagrams (Pearce et al., 1984) show that the Sarcheshmeh-Iju-Meiduk granitoid rocks plot in the field of volcanic arc and Jebal-Barez plots in the field of intraplate granitoids.

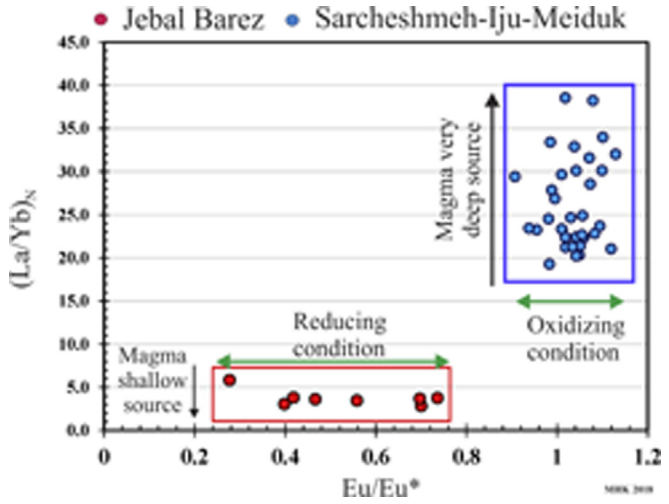

Fig. 8. Plot of (La/Yb)n versus Eu/Eu* indicates that Sarcheshmeh-Iju-Meiduk granitoid rocks originated from a different source than the Jebal Barez granitoids.

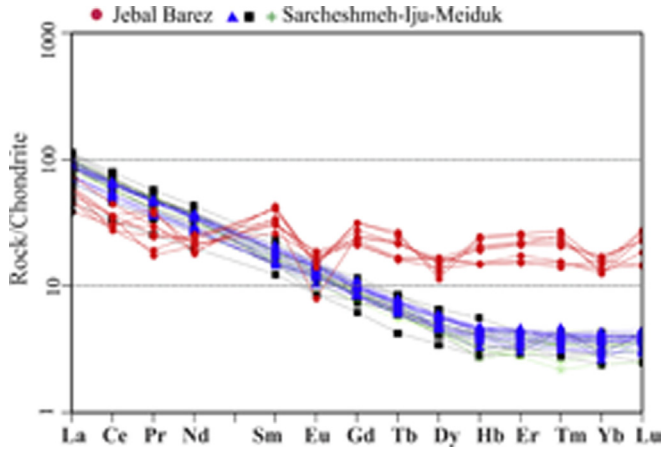

Fig. 9. Chondrite-normalized REE patterns (Boynton, 1984) of Sarcheshmeh-Iju-Meiduk and Jebal Barez granitoids.

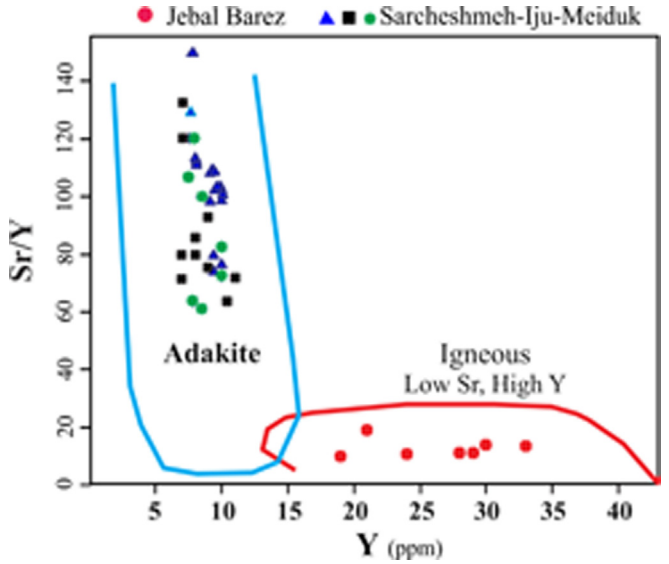

Fig. 10. Plot of Y versus Sr/Y (Defant and Drummond, 1993) shows that Sarcheshmeh-Iju-Meiduk granitoid rocks plot in the field of adakites and Jebal Barez granitoids plot in the field with low Sr and high Y.

Table 5
Rb-Sr & Sm-Nd isotopes (Shafiei et al., 2009).

	$(^{87}Sr/^{86}Sr)i$	Std err. (2σ%)	$(^{143}Nd/^{144}Nd)i$	Std err. (2σ%)
Meiduk deposit	0.70455	0.000006	0.51275	0.000006
Sarcheshmeh	0.704702	0.000008	0.512716	0.000003
Iju deposit	0.704253	0.000007	0.512812	0.000005
Kuh Panj deposit	0.704623	0.000008	0.512653	0.000004
Jebal Barez	0.70681	0.000006	0.512596	0.000004
Sabzevaran	0.705336	0.000006	0.512667	0.000004
Sarduiyeh	0.706153	0.000005	0.512873	0.000005

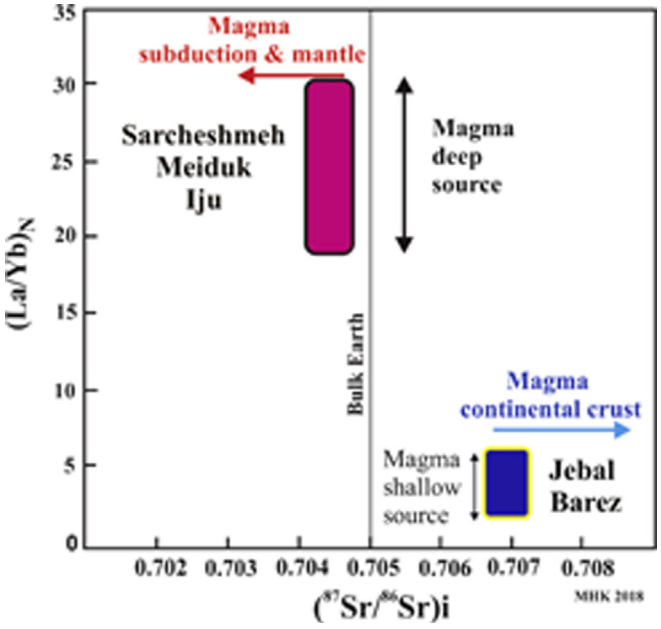

Fig. 11. Plot of Sr-Isotopes versus (La/Yb)n shows that the source and depth of magma for Sarcheshmeh-Iju-Meiduk granitoid rocks differ from Jebal-Barez granitoids.

the subduction zone due to alteration. There are two main areas where oceanic lithosphere can be altered:

1. Oceanic spreading zones: hot oceanic crust formed at spreading centers develops major geothermal cells. There are two main important hydrothermal sources: (1) The geothermal system formed due to cooling of igneous rocks interacting with sea water and (2) magmatic water associated with sub-volcanic intrusions. The first hydrothermal system is very important and creates major alteration zones. They alter mainly the upper part of oceanic crust. Both chrysotile and lizardite form during the alteration of mafic and ultramafic rocks within the oceanic spreading zones (Rüpke et al., 2004). Slower rates of spreading favor alteration. Both olivine and pyroxene are altered to serpentine (chrysotile, lizardite), chlorite, and zeolites.
2. Beginning area of subduction: To begin subduction the oceanic lithosphere must be deflected (Ranero et al., 2005). Major faults form during the deflection of the oceanic lithosphere (Ranero et al., 2005). These faults are very important for channeling the oceanic water to deeper parts of the oceanic lithosphere. As the oceanic water moves along the faults it becomes warmer with increasing depth. Large, hot hydrothermal cells can develop if a) Younger oceanic slabs are warmer and b) Slower rates of subduction. The hydrothermal cells can alter different parts of the oceanic slab. Important hydrated minerals which can form due to alteration are: Chlorites, low temperature serpentine (chrysotile, lizardite), higher temperature serpentine (antigorite), hornblende, etc.

5.2. Dehydration of oceanic slab

The thermal gradient and thermal structure of subducting oceanic lithospheric slabs play an important role in dictating the degree of dehydration at different depths (Peacock and Wang, 1999; Hacker, 2008; van Keken et al., 2011; Magni et al., 2014). The subducting oceanic slabs are classified as hot, warm and cold types based on the thermal gradients (Peacock and Wang, 1999; Hacker, 2008; van Keken et al., 2011). The ages and thermal gradients of an oceanic slab control both rate of subduction and the angle of subducting slab (Wang et al., 2017; Syracuse et al., 2010, Abers et al., 2006; Peacock and Wang, 1999). Old oceanic slabs > 150 Ma (such as Marina Island and NE Japan) are considered as cold with a thermal gradient less than 7 °C/Km, and this type of slabs are thick and much denser. Therefore, the rate of descent of the subducting oceanic slab is high, and the dip of slab is greater than 45°. Oceanic slabs with an age about 45 Ma are warm, with a thermal gradient around 10 °C/Km and finally, young oceanic slabs < 8 Ma (Cascadia, North America and southern Chile), are considered as hot with a thermal gradient greater than 18 °C/Km, thin and less dense, so that the rate of descent of the subducting oceanic slab is low, and the dip of slab is less than 40°.

The geothermal gradient of oceanic slabs at depths of less than 60 km is low (Fig. 12). At depths of more than 60 km, the thermal gradient of the upper part of oceanic lithosphere increases due to hot mantle conversion cells (Fig. 12). At depths of about 100–120 Km, the temperature of the upper part of oceanic lithosphere becomes similar to the upper mantle wedge (Fig. 12). The changes in thermal gradient follow an S-shape curve (Fig. 12). The S-shape is found in the NE Japan oceanic slab (cold slab) and in the Cascadia oceanic slab (warm slab) (Fig. 12).

The relationship between the ages of oceanic slabs, thermal gradients, and depths of dehydration is shown in Fig. 13. Very young oceanic slabs such as that of N. Cascadia (8 Ma) are hot (Fig. 13). The oceanic slab at depths less than 70 Km will be dehydrated (maximum dehydration) (Wada and Wang, 2009). As the age of the subducting oceanic slab increases, the depth of maximum dehydration will increase (Fig. 13). The age of the NE Japan oceanic slab is about 130 Ma (Wada and Wang, 2009) and is a cold type oceanic slab. Maximum dehydration of the NE Japan slab will take place at a much deeper depth (> 150 Km) than that of the N. Cascadia slab (Fig. 13). Subduction rate is

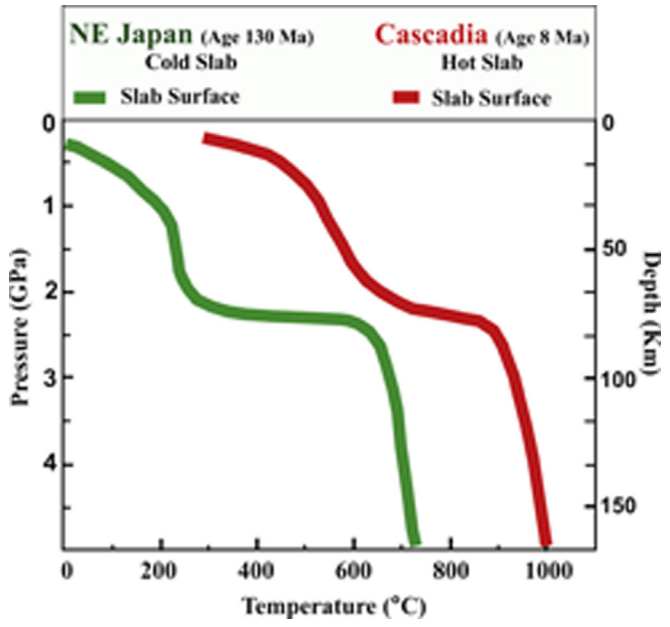

Fig. 12. Thermal gradients of cold and warm oceanic slabs with depth. (Revised after Syracuse and Abers, 2006, Syracuse et al., 2010).

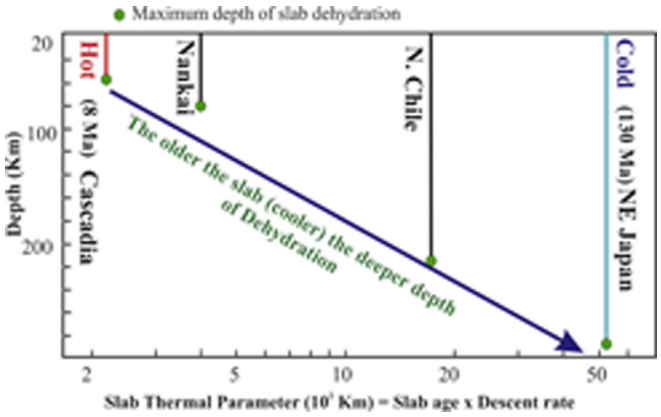

Fig. 13. Depth of dehydration increases with age of oceanic slabs. (Revised after, Wada and Wang, 2009.

directly related to the age of oceanic slabs. The older oceanic slabs (denser) have the higher rate of oceanic descent (Fig. 13). The combination of the age of an oceanic slab and its descent rate are defined as the slab thermal parameter (Fig. 13):

$$\text{Slab Thermal Parameter (100 Km)} = \text{Slab age} \times \text{Descent Rate}$$

Most of the subducting oceanic slabs in South and North America are younger than 45 Ma, therefore, they have warm to hot thermal structures (S. Chile, N. Chile, N. Cascadia, Alaska). The NE Japan and Marina (North America) oceanic slabs are older than 130 Ma and have a cold thermal structure. The slab thermal parameter is higher in NE Japan; so, the depth of dehydration is much deeper in comparison with N. Cascadia which has lower slab thermal parameter (Fig. 13).

Due to prograde metamorphism and dehydration of silicate, water could be released at different depths in the oceanic lithosphere during subduction. Dehydration of the oceanic slab could occur within three depth intervals: (1) Forearc areas; (2) subarc areas, and postarc areas. The thermal structure of oceanic lithosphere would control the quantity of water that could be released from various depth intervals (Alt et al., 2012; Deschamps et al., 2013; Hacker, 2008; Magni et al., 2014; Peacock and Wang, 1999; Rüpke et al., 2004; van Keken et al., 2011).

Serpentine minerals (lizardite, chrysotile and antigorite) are the most important silicates to recycle and carry water and some elements to different depths in the subduction zone (up to 180 km). Temperature and pressure control the geochemistry and type of serpentine minerals. Lizardite and chrysotile are stable at temperatures lower than 300 °C, and are common at shallow depths of subduction zones (Fig. 14a). Lizardite and chrysotile are enriched in Cl, Li, B, Sr, Rb, and Cs. At temperatures above 300 °C lizardite and chrysotile are not stable and are transformed to antigorite. Most Cl, Li, B, Sr, and Rb will be released with some water (Deschamps et al., 2011; Kodolányi and Pettke, 2011; Lafay et al., 2013; Vils et al., 2011). At low pressure, antigorite is stable between temperature 300 and 670 °C (Fig. 14a). Antigorite is the most important and common hydrated mineral in both altered oceanic crust and mantle peridotites. Antigorite contains up to 15–16% of water (average 13 wt%). Fluids released from antigorite have high ratios of B/La, B/Nb, B/Th, U/Th, Sb/Ce and Sr/Nd (Deschamps et al., 2011). The general formula of antigorite is as follows:

$$(Mg,Fe,Ni,Al,Mn,Zn)_{2-3}(Si,Al,Fe)_2O_5(OH,Cl,F)_4$$

Field of stability of serpentine minerals was studied by Bromiley and Pawley (2003) and Ulmer and Trommsdorff (1995). The depth of antigorite breakdown depends on the thermal gradient of the oceanic slab:

Cold oceanic slab, if the thermal gradient of an oceanic slab is less than 7 °C/Km, at a depth of about 140 Km and temperature of around 650 °C, antigorite breaks down to forsterite + enstatite and water (Fig. 14a, cold oceanic slabs (C)).

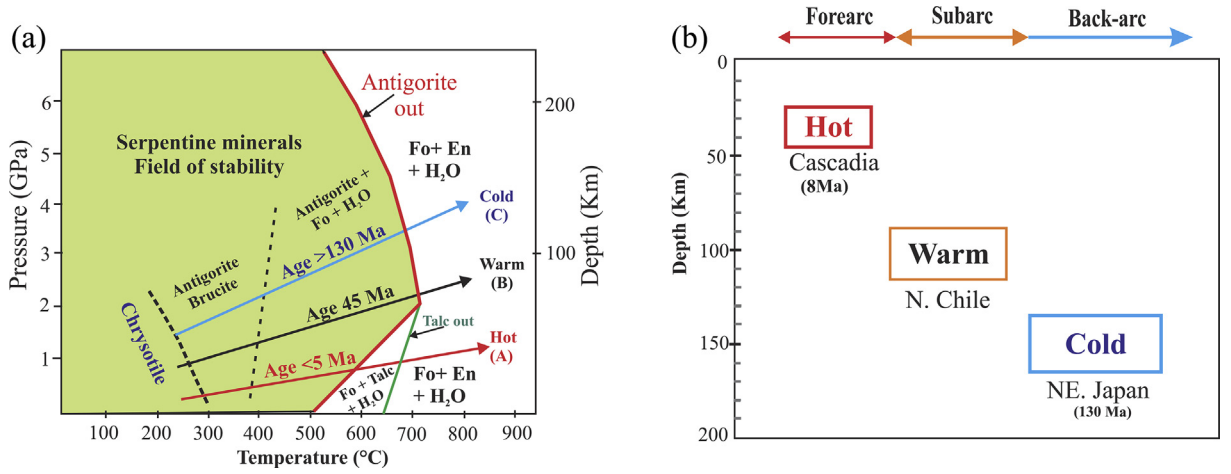

Fig. 14. (A) The stability field and dehydration of antigorite and talc within different oceanic slab thermal gradients. Mineral stabilities are from Bromiley and Pawley (2003) and Ulmer and Trommsdorff (1995), Perrillat et al. (2005), Wunder and Schreyer (1997). (B) Depth of maximum dehydration of oceanic slab for three cases of hot, warm, and cold conditions.

Warm oceanic slab, if the thermal gradient of an oceanic slab is between 9 and 15 °C/Km, at a depth of about 80–120 Km and temperature of around 670–700 °C, antigorite breaks down to forsterite + enstatite and water (Fig. 14a, warm oceanic slabs (B)).

Hot oceanic slab, if the thermal gradient of an oceanic slab is less than 20 °C/Km (Fig. 14a, hot oceanic slabs (A)), at a depth of about 35 Km and temperature of around 570 °C, antigorite breaks down to forsterite + talc and water, according to the following reaction:

$$5Mg_3Si_2O_5(OH)_4(\text{antigorite}) = 6MgSiO_4(\text{forsterite}) + Mg_3Si_4O_{10}(OH)_2(\text{talc}) + 9H_2O(\text{fluid})$$

Some of the water will be carried with talc to greater depths (Fig. 14a). At a depth of about 40 km and temperature of around 680 °C talc will break down to forsterite and enstetite:

6Forstrite + Talc = 5Forsterite + 5Enstetite + H_2O (Fluid) (Fig. 14a) (Perrillat et al., 2005; Wunder and Schreyer, 1997). As a result, in a hot oceanic slab, talc and all the serpentine minerals such as lizardite, chrysotile and antigorite will be dehydrated, and water will be released within the ***forearc depth* (*30–50 km,*** Fig. 14b). This fluid could migrate along major faults to the continental crust with no magmatic events, while in a warm oceanic slab, antigorite and talc could be dehydrated and water could be released within the ***arc at depth* (*80–130 km,*** Fig. 14b). These fluids are very important to decreasing the melting point of rocks and causing magmatism.

The roles of water and magmatism within different depths of subduction are shown in Fig. 15(a) and (b) (more details can be found in Grove et al., 2012). In the case of (A), at depths of about 40 km (Fig. 15a, point L) and a temperature of 850 °C (Fig. 15b, point L) fluid which was released from the oceanic slab has a lower melting point than the mantle wedge. At point L, the oceanic slab will begin to partially melt, and a small amount of magma will be generated. As the magma is ascending then it will move to lower temperature (< 700 °C) and the magma therefore will be solidified and cannot migrate a long distance. In the case of (B), at a depth of about 80 km (Fig. 15a, point M) and temperature of 900 °C (Fig. 15b, point M) more water will be released due to the dehydration of silicates in the oceanic slab. The oceanic slab will began partially melting and more magma will be generated. The magma will pass through hotter mantle and the temperature of magma will increase up to 1200 °C (Fig. 15a). This magma can react and partially melt mantle or continental crust. This magma can reach to the surface and solidify as volcanic and/or plutonic rocks. At greater depth and higher temperature, higher volumes of magma can be generated (Fig. 15a). In the case of (C), at depths of about 125 Km (Fig. 15a, point N), there is no hydrated silicate to provide the water (Fig. 15b, point C) and therefore no magmatism can be initiated beyond this depth.

6. Discussion

The source of porphyry copper deposits is mostly I-type intermediate granitoid rocks. These granitoids (unaltered rocks) have magnetic susceptibilities > 300×10^{-5} SI and therefore belong to the magnetite-series (oxidized magma). The ratio of Eu/Eu* of granitoids is used to estimate the oxidation state of granitoid rocks. If the ratio of Eu/Eu* is greater than one then the granitoid is considered as an oxidized type. High magnetite content within the potassic altered zone of porphyry copper deposits is considered as a good indicator that the oxygen fugacity of the magmatic water was high. High oxygen fugacity has an important role in the formation of porphyry copper deposits (Candela, 1992; Ballard et al., 2002; Mungall, 2002; Richards, 2003, 2011; Liang et al., 2006; Li et al., 2012; Han et al., 2013; Wang et al., 2014; Zhang et al., 2014; Shen et al., 2015; Wu et al., 2016; Sillitoe, 2010; Cao et al., 2016, 2017; Sun et al., 2013, 2015, 2017).

Based on experimental research by Trail et al. (2012) on zircon, it was suggested that the ratio of Ce^{4+}/Ce^{3+} is controlled by oxygen fugacity and temperature (the higher ratio indicates higher oxygen fugacity). Higher ratios of Ce^{4+}/Ce^{3+} indicate higher oxygen fugacity of the magma (Smythe and Brenan, 2015, 2016; Trail et al., 2012). The ratio of Ce^{4+}/Ce^{3+} in zircon in 13 ore-bearing intrusions associated with 9 porphyry copper deposits in the Central Asian metallogenic belt was ranged from 29 to 592 (Shen et al., 2015). Based on this study, the ratio of Ce^{4+}/Ce^{3+} in zircons from large porphyry copper deposits is between 74 to 592, intermediate deposits is 74 to 332 and small deposits is 28 to 158. According to Shen et al. (2015), the ratio of Ce^{4+}/Ce^{3+} approximately equal to 120, can discriminate between granitoids associated with small porphyry copper and large-intermediate deposits. The Ce^{4+}/Ce^{3+} ratios of non-mineralized I-type (Kosciusko) and S-type (Berridale adamellite) from the Lachlan fold belt in Australian range from 0.54 to 2.53 (Shen et al., 2015). Smythe and Brenan (2016) determined the oxygen fugacity during zircon crystallization to be between FMQ −1.0 and +2.5 (where FMQ is the fayalite–magnetite–quartz buffer).

The ratio of Ce^{4+}/Ce^{3+} in zircons from Dexing porphyry Cu deposit in China was studied and compared with other porphyry deposits of the world (Zhang et al., 2017). Based on this study the calculated oxygen fugacity of zircons from ore-bearing granitoids lies between DFMQ + 0.5 to DFMQ + 3.5. El Teniente, world's largest porphyry Cu deposit average has DFMQ + 2.5 (Zhang et al., 2017). Zircons from

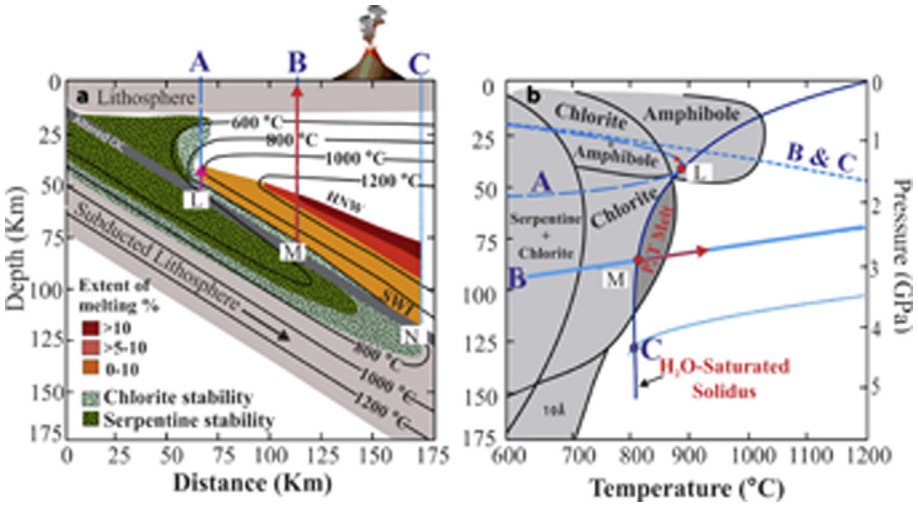

Fig. 15. These two diagrams are from Grove et al. (2012). (a) A typical cross section through a subduction zone using the thermal model from Grove et al. (2009) for a slab dip of 30° and a convergence rate of 40 km per million years. Also shown are the stability limits for high-H_2O (> 10 wt%) minerals. (b) Phase with the temperature-depths paths from panel a superimposed. The dark gray region labeled P, Tmelt shows the region of pressure-temperature space where the stability of hydrous phases at the base of the mantle wedge allows H_2O-saturated melting to begin. Figure with minor modifications from Grove et al. (2009). Abbreviations: HNW, hot nose of the wedge; OC, oceanic crust; SWI, slab-wedge interface.

Table 6
Partition coefficient of copper between silicates-melt and sulfides-melt (Lee et al., 2012).

Olivine	Orthopyroxene	Clinopyroxene	Amphibole	Spinel	Garnet	Sulfides
0.048	0.034	0.043	0.05	0.22	0.0035	800

barren granitoids have low oxygen fugacity and were less than DFMQ − 1 (Zhang et al., 2017). There is no precise agreement about the oxygen fugacity for large-intermediate and small size porphyry copper deposits. Sun et al. (2013), proposed that ΔFMQ +2 to +4 is the most favorable range of oxygen fugacity for porphyry deposits, but others suggested that ΔFMQ + 2 is a good number (Mungall, 2002). The partition coefficient of copper as a chalcophile element is very high for sulfur in comparison with silicates (Table 6). Sulfur is very important for controlling the copper content of the magma. Sulfate is 10 times more soluble than sulfide (Sun et al., 2015; Simon et al., 2006, 2008). With high oxygen fugacity and the higher sulfate content, more sulfur and copper will be partitioned in the magma. When the FMQ is in the fayalite–magnetite–quartz oxygen buffer, most of sulfur in the magma is present as sulfate (Sun et al., 2015). In the case of high oxygen fugacity (higher than AFMQ + 2), the solubility of sulfur increases from 1000 ppm to 1 wt% (Sun et al., 2015).

Partial melting of oceanic slab, mantle peridotite and lower crust under different oxygen fugacity are plotted in Fig. 16. Partition coefficients of Cu, silicates and sulfides are reported in Table 6. Copper is very incompatible in garnet and highly compatible in sulfides (Table 6). Rock containing garnet with a small degree of partial melting, will produce magma, enriched in copper. Partial melting of oceanic slab under three different oxygen fugacity DFMQ + 0, DFMQ + 1, to DFMQ + 1.5. is plotted in (Fig. 16). At an oxygen fugacity of DFMQ + 1.5, and partial melting between 10 and 30 percent, magma has a higher Cu content (Table 7). At 17% partial melting, the Cu content of magma is 380 ppm (Fig. 16; Table 7). At low degrees of partial melting of mantle peridotite and lower crust (with less than 8% melting), more Cu will partition in the magma at higher oxygen fugacity conditions (Fig. 16; Table 7). Mantle peridotite does not have sufficient copper to form a porphyry copper deposit (Lee et al., 2012). Due to metasomatism, mantle wedge peridotite can be enriched in copper. Magma originating from less than 10% partial melting of the metasomatized mantle peridotite under highly oxidizing conditions can form a porphyry copper deposit. Magma originating from 15 to 25% of partial melting of oceanic slab under oxygen fugacity DFMQ + 1.5, is the best candidate to form a porphyry copper deposit (Fig. 16; Table 7).

The concentration of several porphyry copper deposits within a small portion of the UDMB indicates that Neo-Tethys subducted oceanic

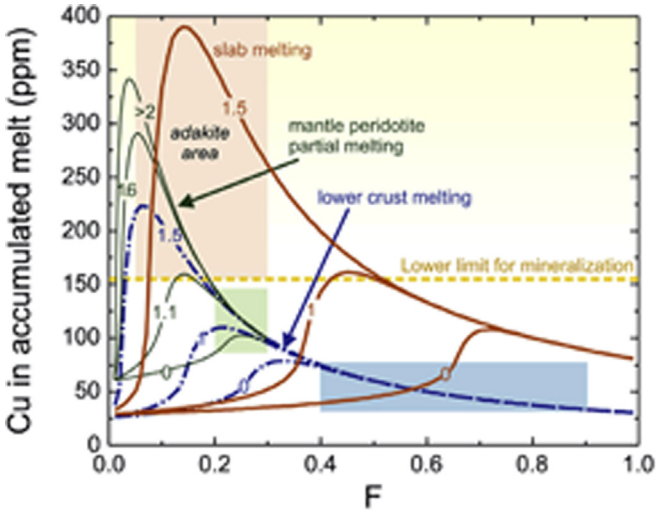

Fig. 16. The Cu content in the accumulated melt during partial melting as a function of degree of melting (F) under different oxygen fugacity. Red lines and blue dash-dot lines represent slab and lower crust melting models, respectively, varied from DFMQ + 0, DFMQ + 1, to DFMQ + 1.5. Mantle wedge partial melting in green lines of Lee et al. (2012) is compared to slab and lower crust partial melting. The pink and light blue shadows highlight the Cu concentration area at the partial melting degree to produce the Sr/Y and La/Yb characteristics of adakite. The green shadow highlights the Cu concentration areas from mantle wedge partial melting to form an arc magma. The yellow dash line and shadow represent the lower limit of Cu concentration and range essential for mineralized porphyry magma. Only slab melts satisfy the condition to generate a Cu mineralized porphyry (Zhang et al., 2017). (For interpretation of the references to colour in this figure legend, the reader is referred to the web version of this article.)

slab had special features for the formation of porphyry copper deposits along the Kerman belt. The granitoid rocks within KDCB were intruded during Miocene time (18.82–9.2 Ma), but the Jebal Barez granitoids are Late Oligocene in age. Based on trace element discrimination diagrams, the tectonic setting of granitoids within Kerman belt are volcanic arc, while Jebal Barez granitoids are within an intraplate setting. The ratio

Table 7
Data in table are extracted from diagram in Fig. 16 (Zhang et al., 2017, White and Klein, 2013, Rudnick and Fountain, 1995).

Rock Types	Cu & S (ppm) Content	Oxygen Fugacity	Partial Melting At Maximum Cu	Cu (ppm) In Magma
Oceanic Slab	Cu =70 S= 1000 (White and Klein, 2014).	0	70	120
		1	45	160
		1.5	10	300
			17	380
			30	300
Mantle Wedge peridotite	Cu =40 S = 500	0	23	100
		1.1	17	160
		1.6	5	280
		>2	4	340
Lower Crust	Cu =30 S = 400 Rudnick and Fountain (1995)	0	30	60
		1	20	110
		1.5	5	225

of Eu/Eu^* of granitoid rocks from Kerman belt are higher than 1.2, therefore magma was formed under oxidizing conditions. But the ratio of Eu/Eu^* is less than 0.7 in Jebal Barez granitoids and magma formed under reducing conditions. The ratio of Sr/Y for Kerman granitoids is greater than 60, therefore they are adakite type and Jebal Barez is less than 20. The ratio of (La/Yb)n for the Kerman granitoid rocks is between 17 and 35, therefore that magma was generated from a deep source, but the ratio for the Jebal Barez granitoids is less than 7 and magma was generated at shallower depth. Based on the $(^{87}Sr/^{86}Sr)i = 0.704–0.705$, magmas for Kerman belt granitoids originated from the subduction zone, but the ratio of $(^{87}Sr/^{86}Sr)i > 0.707$ for Jebal Barez granitoids suggests they originated from the continental crust. Since magma for Jebal Barez granitoids originated from the continental crust under reducing conditions (Fig. 16; Table 7), and the copper content of the magma was around 30 ppm; this magma did not have enough copper and geochemically was not suitable for the formation of porphyry copper deposits.

Different sections of the Neo-Tethys subducted oceanic slab had unique and special features which resulted in changes of magmatism and formation of ore deposits. Subducted Neo-Tethys oceanic slab which formed the KPCB had the following features:

1. Subducted oceanic slab was warm-cold, thermal gradient of the oceanic slab was between 8 and 12 °C/Km (Fig. 17). This was very important, because smaller amounts of fluids were liberated at the ***forearc depths*** (depth 30–50 Km, Fig. 18) and more than 90% of all the water within the oceanic slab was released within the ***subarc region*** (depth of 100–130 Km, Fig. 18). Water caused the melting temperature of the rocks to become very low, therefore magma with fluid was generated. The amount of water that was released had an important and significant role in the degree of partial melting. This type of magma with high fluid content and an appropriate amount of copper was important in the formation of porphyry copper deposits within the Kerman belt.
2. There are some portions of the UDMB, where the subducted ocean slab was hot (thermal gradient of the oceanic slab was more than 18 °C/Km) and more than 90% of the water was released within the ***forearc depth***. Only minor amounts of water was delivered to depth of the ***subarc***. In these portions of the UDMA, there is no porphyry copper deposit (Fig. 17). In this portion of the belt, Pb-Zn MVT deposits were formed (Karimpour and Sadeghi, 2018).
3. Magma generated under high oxygen fugacity of DFMQ + 1.5. It has been proposed that the formation of a porphyry deposit is closely related to the presence of a highly oxidized magma (Sun et al., 2013, 2014a,b, 2015, 2017; Zhang et al., 2017). Based on the following facts, oxygen fugacity is not very significant for the formation of porphyry copper deposits:
   - There are a lot of I-type granitoid (magnetite series, oxidized type) with no alteration and no mineralization.
   - In each porphyry copper deposit, usually there are a dozen sub-volcanic intrusions (I-type granitoid, magnetite-series) which are responsible for the formation of porphyry copper deposits. Multiple intrusion episodes of these granitoids is about 2 million years. Among these sub-volcanic rocks, there are at least two intrusive granitoids which are not mineralized. These two granitoids have very low magmatic water. They are considered as destructive, because they increase the ratio of waste/ore. The barren granitoid rocks (diorite, quartz diorite, and monzonite) have more magnetite in comparison with the mineralized one. There is an important question, if highly oxidized magma is very important for the formation of porphyry copper deposits? and why are these highly oxidized granitoids not mineralized?
4. Based on the following evidences, the depth where magmas are forming within the subduction zones, do not control the fertility and based on the ratio of Sr/Y > 25 of igneous rocks which is being proposed by Wan et al. (2018) and Deng et al. (2018); it is not possible to discriminate between barren and ore related magma:
   - In porphyry copper deposits around the world during the period of mineralization and magmatism (which is around 1.5 million years) more than seven sub-volcanic rocks, monzonite, quartz monzonite, diorite and quartz diorites have been formed (Sillitoe, 2010; Golestani et al., 2018; Karimpour et al., 2012; Malekzadeh Shafaroudi et al., 2015). A comparation on Sr/Y ratio on the sub-volcanic rocks (e.g. Sarcheshmeh and Iju porphyry copper deposit), revealed that the ratio of Sr/Y is > 50 in both cases and it is the same in mineralized and non-mineralized sub-volcanic rocks, formed during the time interval of mineralization.
   - Both Sarcheshmeh and Iju porphyry copper deposits have similar Ratios of Sr/Y > 60 and (La/Yb)N > 20. Magmas for both originated from subducted oceanic slab in a very deep section. In both deposits, the magma was generated from similar depth, but Sarcheshmeh is a giant deposit while Iju is very small and low grade (Table 4).
   - In Eastern Iran, near Gonabad city, there are some granitoids with adakitic characteristics (ratio of Sr/Y > 60 and (La/Yb)N > 20) within the Lut Block, Eastern Iran (Moradi Noghondar et al., 2012). The magma for these granitoids originated from a very deep source in the subduction zone, during Eocene time (39 Ma). These granitoids are not mineralized. In the same region within the Lut Block, Eastern Iran (Malekzadeh Shafaroudi et al., 2015), there are some granitoids which originated from a shallower depth (ratio of Sr/Y < 40 and (La/Yb)N < 10) in the subduction zone (39.8 Ma). These granitoids are the source of Maherabad and Shadan porphyry Cu-Au deposits (Malekzadeh Shafaroudi et al., 2015).
5. The water content of the oceanic slab for the formation of each porphyry copper deposit along the Kerman belt was different.
6. Partial melting of the oceanic slab for large deposits was between 25 and 30 percent.
7. The sulfur content of the oceanic slab was more than 700 ppm and copper content were about 70 ppm.
8. As this magma reached near the surface, magmatic water carrying Cu and other elements as chloride complexes under special conditions, porphyry copper deposits were formed.

In early stages of subduction, the continental crust was thinner. During Eocene time, magma originated from partial melting of the mantle wedge above the oceanic slab, could reach the surface and produce volcanic rocks. Eocene andesite, dacite, and rhyodacite are reported as various types of pyroclastics and lavas. Since the copper content of the mantle wedge was low, these magmas did not have

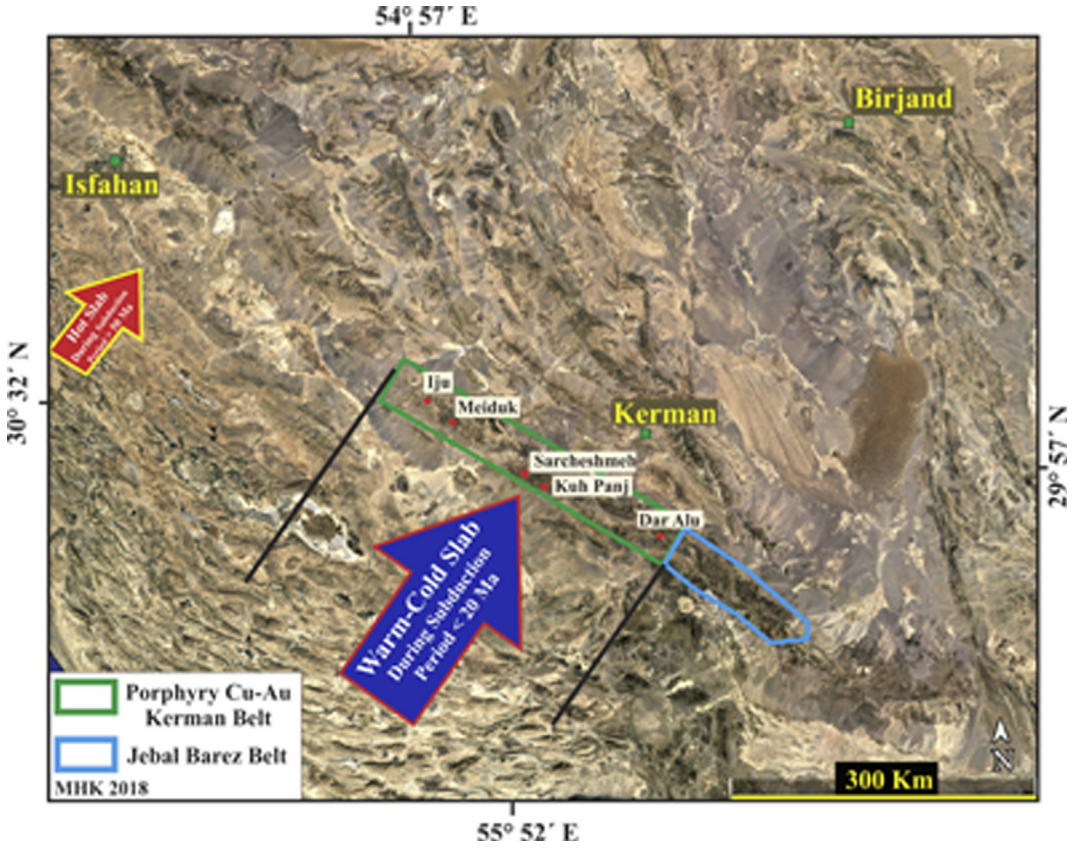

Fig. 17. Location of the KPCB and Jebal Barez belt, cold-warn and hot oceanic slabs are plotted on Google Earth Map.

sufficient copper to form porphyry copper deposits. From Early Eocene till late Miocene time, due to compressional tectonics (folding and thrusting) and magmatism (formation of new crust), the continental crust became much thicker (Agard el al., 2011; Fakhari et al., 2008; Mouthereau et al., 2012; Pirouz et al., 2017). Magma originated from partial melting of the oceanic slab, during the Miocene, solidified at depth. The type of magma which was formed during Miocene time was very important for the formation KPCB. In the following section, the process which was involved for the formation of magmas will be explained.

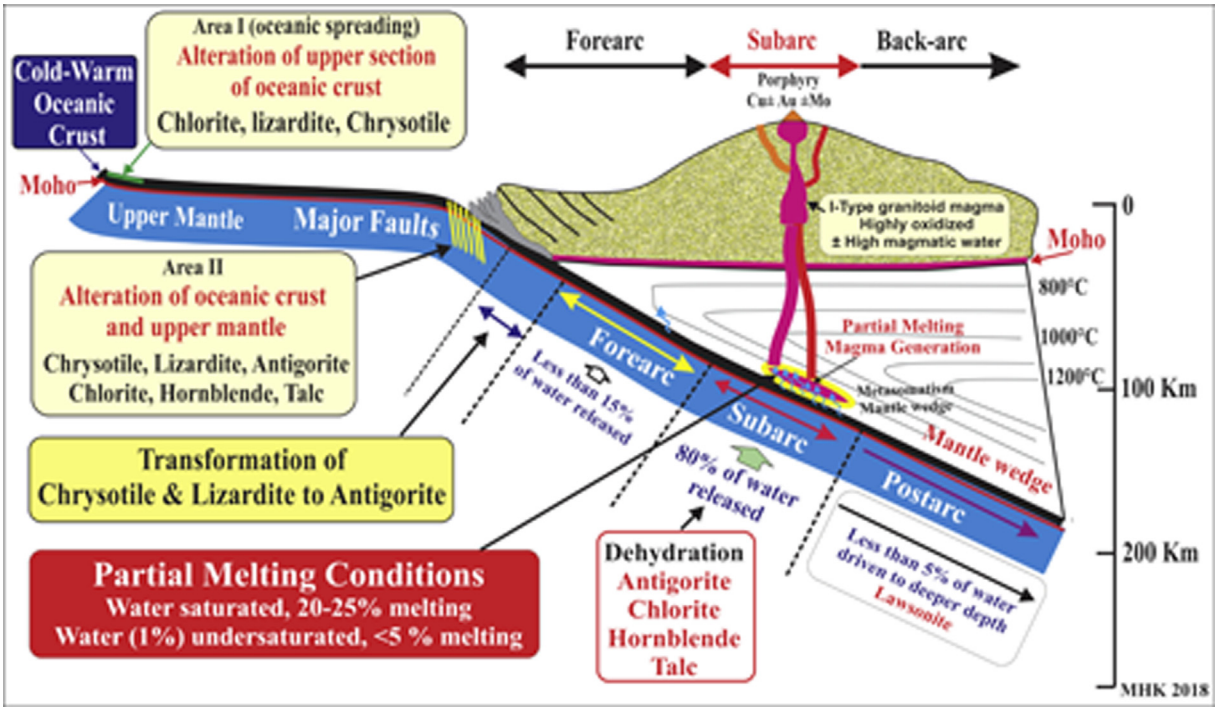

Fig. 18. Cold-Warm oceanic slab dehydrates and releases most of its water within the subarc region.

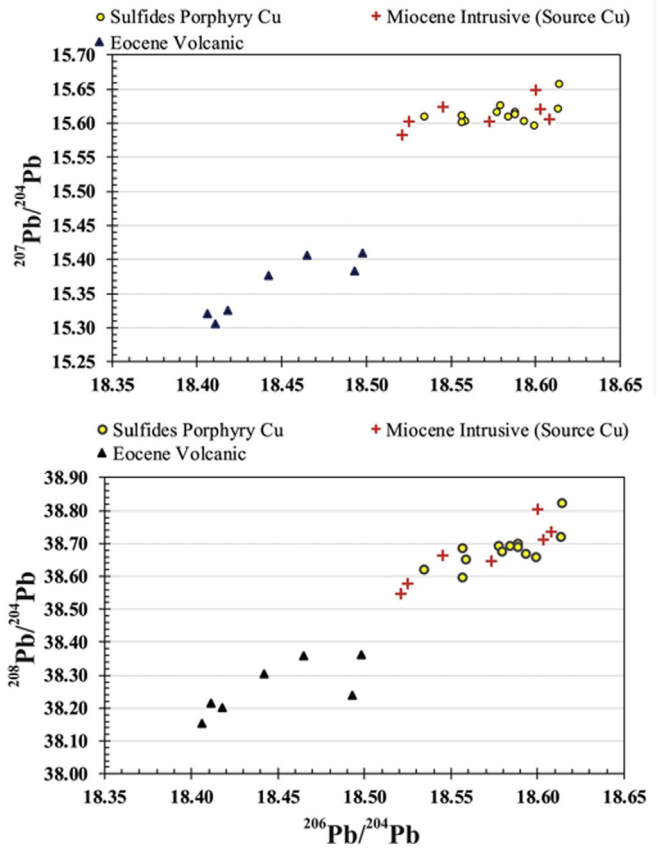

Fig. 19. Pb-isotopes composition of Eocene volcanic rocks along Kerman belt, porphyry copper deposits (sulfide minerals) and the granitoid rocks (the source of porphyry copper deposits) along Kerman belt.

Pb-isotope compositions of Tertiary volcanic rocks, Miocene granitoid rocks (the source of porphyry copper deposits along Kerman belt), and porphyry copper deposits (sulfide minerals) along the Kerman belt, are plotted in Fig. 19 (Shafiei, 2010; Shahabpour and Kramers, 1987). Trace elements and isotopic composition of Eocene volcanic rocks along the Kerman belt are typical of a subduction-related setting. These volcanic rocks were formed sometimes at the early stage of subduction.

The Pb-isotope compositions of Eocene volcanic rocks are low radiogenic, therefore minor crustal contamination (Fig. 19). The Pb-isotopes composition of both porphyry copper deposits and the granitoids (source rocks) are similar (Fig. 19). Based on the geochemistry of trace elements, REE and Rb-Sr isotopes composition (The ratio of (La/Yb)n is between 17 and 35, Sr/Y > 60, ($^{87}Sr/^{86}Sr$)i = 0.7041) granitoid magma originated from a deep source in the subduction zone. From Early Eocene till late Miocene, the Pb-isotope composition of the continental crust became more radiogenic (higher $^{206}Pb/^{204}Pb$ and $^{208}Pb/^{204}Pb$). During this period, due to active tectonics, the continental crust became thicker. Pb-isotopes composition of porphyry copper deposits and the Miocene granitoid rocks are more radiogenic in comparison with the Eocene volcanic rocks (Fig. 19). Pb-isotopes composition and thickness of continental crust during the Miocene were different in comparison with Early Eocene time (higher radiogenic Pb-isotopes and thicker). As the granitoid magma was contaminated in the continental crust during Miocene time, they got higher radiogenic Pb-isotopes.

Water content of subducted oceanic slab played an important role for the formation and size of the porphyry coper deposits along the Kerman belt. The initial melting point of mantle wedge peridotite or oceanic slab basalt at a depth of 100 Km, in dry conditions, is around 1200–1400 °C. Under water saturated conditions, the melting point dropped to less than 800 °C. The initial melting point in the case of

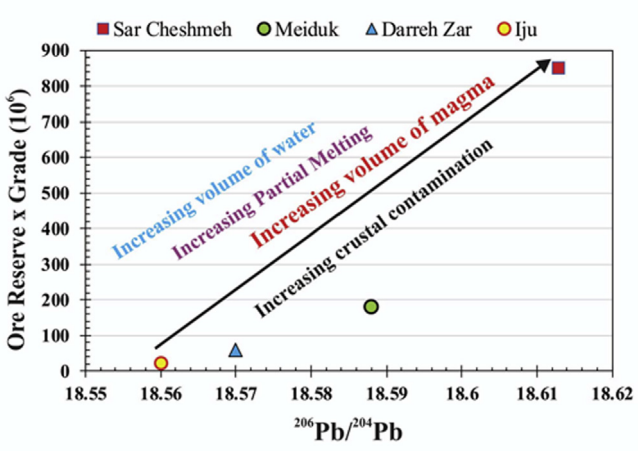

Fig. 20. Pb-isotope compositions of porphyry copper deposits along the Kerman belt versus ore grade × grade 10^6.

under-saturated conditions is more than 1000 °C (Green, 1973; Kushiro, 1974; Novella et al., 2017). The melting temperature at a depth of 100 Km is a function of water content. The higher water content causes the lower melting temperature. High degrees of partial melting are related to higher water available at the melting region.

The $^{206}Pb/^{204}Pb$ composition of porphyry copper versus ore grade × grade (10^6) are plotted in Fig. 20. It is very important to notice that there is a good correlation between $^{206}Pb/^{204}Pb$ ratio and ore reserves (Fig. 20). Sarcheshmeh porphyry copper deposit has higher radiogenic $^{206}Pb/^{204}Pb$ in comparison with Iju and other relatively smaller porphyry copper deposits (Fig. 20). Trace elements, REE, and isotopic composition (explained earlier) of the granitoids indicate that the magma for all these deposits originated within a deep source in the subduction zones. The main difference was the degree of partial melting. In the case of Sarcheshmeh porphyry copper deposits, the subducted oceanic slab was enriched in water. More than 80% of the slab water was released at depth of around 110 to 130 Km. Higher water contents lowered the melting temperature of oceanic slab and due to a high degree of partial melting (20–25%) a large volume of magma was generated. The water content of this magma was very high. High volumes of magma (Sarcheshmeh) could melt more continental crust materials, therefore it has higher radiogenic $^{206}Pb/^{204}Pb$ (Fig. 20). Pb-isotope compositions of porphyry copper deposits along the Kerman belt versus Rb-Sr isotopes also show a good correlation between $^{206}Pb/^{204}Pb$ and Sr-isotopes (Fig. 21). High volumes of magma (Sarcheshmeh) could melt more continental crust materials, therefore it

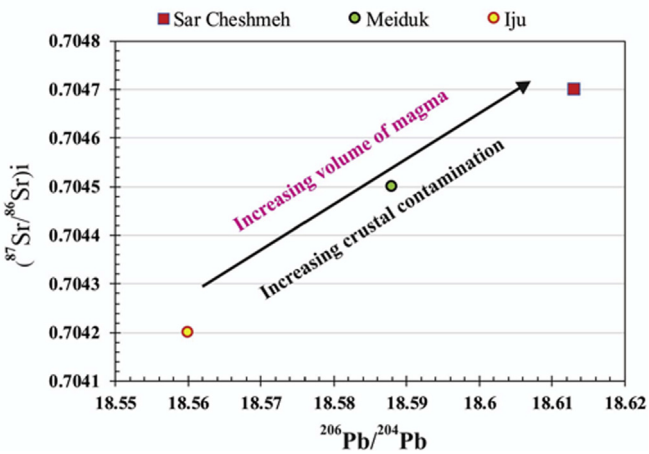

Fig. 21. Pb-isotope compositions of porphyry copper deposits along the Kerman belt versus Rb-Sr isotopes.

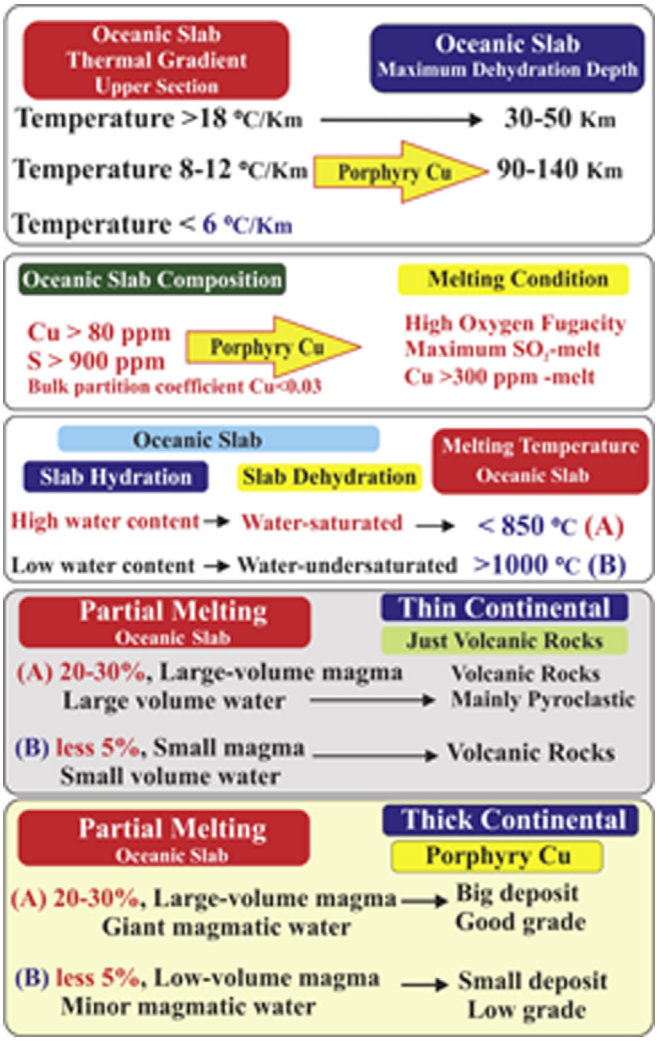

Fig. 22. Important features and processes within the subduction zones controlling the formation and size of porphyry copper deposits.

has higher radiogenic ($^{87}Sr/^{86}Sr$)i (Fig. 20). Large volumes of magmas with high magmatic water were very important for the formation of Sarcheshmeh porphyry copper deposit.

In the case of Iju (small size and low-grade deposit), the water content of the subducted oceanic slab was low. Minor water at a depth of 110–130 Km lowered the melting temperature of the oceanic slab for a low degree of partial melting (less than 5 percent). Low volumes of magma resulted in very low contamination in the crust, therefore it has low radiogenic $^{206}Pb/^{204}Pb$ (Fig. 20). Small volumes of the magma and low magmatic water formed Iju porphyry copper deposit (small size and low-grade deposit).

7. Conclusion

There are two granitoid belts within the southern part of The UDMA, western part of the Kerman town, the Sarcheshmeh granitoids and the Jebal-Barez granitoids. These two granitoid belts have different tectonic settings and they have major differences regarding petrogenesis.

It is also not possible to discriminate between barren and ore-related magma using Sr/Y and La/Yb ratios. The mineralized (Maherabad and Shadan porphyry Cu-Au deposits) and non-mineralized granitoids (Gonabad) in the Lut Block show similar ratios of Sr/Y and La/Yb. In the KPCB both the Sarcheshmeh and Lju deposits have similar ratios of Sr/Y > 60 and (La/Yb)n > 20 while they show different tonnage and grade.

The type of magma which was formed during Miocene time was very important for the formation of the KPCB. Pb and Sr isotope data indicate that the subducted oceanic slab was not similar for the formation of Sarcheshmeh and Iju porphyry Cu deposits. The main differences were the water content of the slabs, the thermal gradient of the slabs (between 8 and 12 °C/Km), the chemical and mineralogical composition of the slabs, and the rate of subduction. For the formation of porphyry copper deposits, a warm-cold subducted oceanic slab with a thermal gradient between 8 and 12 °C/Km was needed. Within the subarc region (i.e. 100–130 km) more than 90% of all the water within the oceanic slab was released which controlled the degree of partial melting.

Important parameters which control the formation, size and grade of porphyry copper deposits are shown in Fig. 22 and summarized as follows:

- Deep oceanic slab thermal gradient (upper surface) with 8–10 °C/Km
- High water content of oceanic slab
- Maximum depth of dehydration might be deeper than 90 Km
- Dehydration of the oceanic slab (about 80%) may occur within a narrow depth interval.
- The degree of partial melting might be about 20–25% (higher content of water may reveal lower melting temperature and favor partial melting)
- Chemical and mineralogical composition of the oceanic slab or mantle wedge (source rocks) may contain Cu > 70 ppm, S > 100 ppm. Cu and S should be incompatible in source rocks.
- And finally, the condition for melting include; high oxygen fugacity, maximum dehydration, high amount of water, and 20–25% partial melting generating a significant amount of magma where most of the copper and sulfur may partition.

Acknowledgment

The authors wish to thank E. Lynch for comments on early version of this manuscript and P.K. Holmes for English correction of the manuscript. Two anonymous reviewers are thanked for constructive comments on the manuscript. Dr. Hooshang Asadi Haroni is acknowledged for the handling and review of this manuscript.

References

Abdi, M., Karimpour, M.H., 2013. Petrochemical characteristics and timing of middle Eocene granitic magmatism in Kooh-Shah, Lut Block, Eastern Iran. Acta Geol. Sin. 87 (4), 1032–1044. https://doi.org/10.1111/1755-6724.12108.

Abers, G.A., van Keken, P.E., Kneller, E.A., Ferris, A., Stachni, J.C., 2006. The thermal structure of subduction zones constrained by seismic imaging: Implications for slab dehydration and wedge flow. Earth Planet Sci. Lett. 241, 387–397. https://doi.org/10.1016/j.epsl.2005.11.055.

Agard, P., Omrani, J., Jolivet, L., Mouthereau, F., 2005. Convergence history across Zagros (Iran): constraints from collisional and earlier deformation. Int. J. Earth Sci. 94, 401–419. https://doi.org/10.1007/s00531-005-0481-4.

Agard, P., Omrani, J., Jolivet, L., Whitechurch, H., Vrielynck, B., Spakman, W., Monié, P., Meyer, B., Wortel, R., 2011. Zagros orogeny: a subduction-dominated process. Geol. Mag. 148, 692–725. https://doi.org/10.1017/S001675681100046X.

Aghazadeh, M., Hou, Z., Badrzadeh, Z., Zhou, L., 2015. Temporal-spatial distribution and tectonic setting of porphyry copper deposits in Iran: constraints from zircon U-Pb and molybdenite Re-Os geochronology. Ore Geol. Rev. 70, 385–406. https://doi.org/10.1016/j.oregeorev.2015.03.003.

Ahmadian, J., Haschke, M., McDonald, I., Regelous, M., RezaGhorbani, M., Emami, M.H., Murata, M., 2009. High magmatic flux during Alpine-Himalayan collision: constraints from the Kal-e-Kafi complex, central Iran. Bull. Geol. Soc. Am. 121 (5–6), 857–868. https://doi.org/10.1130/B26279.1.

Alaminia, Z., Karimpour, M.H., Homam, S.M., Finger, F., 2013. The magmatic record in the Arghash region (northeast Iran) and tectonic implications. Int. J. Earth Sci. 102 (6), 1603–1625. https://doi.org/10.1007/s00531-013-0897-1.

Alavi, M., 2004. Regional stratigraphy of the Zagros fold-thrust belt of Iran and its proforeland evolution. Am. J. Sci. 304, 1–20. https://doi.org/10.2475/ajs.304.1.1.

Alavi, M., Mahdavi, M.A., 1994. Stratigraphy and structure of the Nahavand region in western Iran and their implications for the Zagros tectonics. Geol. Mag. 131, 43–47.

Alavi, M., 2007. Structures of the Zagros fold–thrust belt in Iran. Am. J. Sci. 307, 1064–1095. https://doi.org/10.2475/09.2007.02.
Almasi, A.R., Karimpour, M.H., Hattori, K., Santos, J.F., Ebrahimi, K., Rahimi, B., 2017. Au-bearing magnetite mineralization in Kashmar (alteration, mineralization, geochemistry, geochemistry and fluid inclusions); and Tectono-magmatism of northeast of Iran. J. Econ. Geol. 8 (2) ISSN 2008-7306.
Alt, J.C., Shanks, W.C., Bach, W., Paulick, H., Garrido, C.J., Beaudoin, G., 2007. Hydrothermal alteration and microbial sulfate reduction in peridotite and gabbro exposed by detachment faulting at the Mid-Atlantic Ridge, 15°20′N (ODP Leg 209): a sulfur and oxygen isotope study. Geochem., Geophys., Geosyst. 8 (8). https://doi.org/10.1029/2007GC001617.
Alt, J.C., Garrido, C.J., Shanks, W.C., Turchyn, A., Padrón-Navarta, J.A., López Sánchez-Vizcaíno, V., Marchesi, C., 2012. Recycling of water, carbon, and sulfur during subduction of serpentinites: a stable isotope study of Cerro del Almirez, Spain. Earth Planet. Sci. Lett. 327–328, 50–60. https://doi.org/10.1016/j.epsl.2012.01.029.
Arjmandzadeh, R., Santos, J.F., 2014. Sr-Nd isotope geochemistry and tectonomagmatic setting of the Dehsalm Cu-Mo porphyry mineralizing intrusives from Lut Block, eastern Iran. Int. J. Earth Sci. 103 (1), 123–140. https://doi.org/10.1007/s00531-013-0959-4.
Arjmandzadeh, R., Karimpour, M.H., Mazaheri, S.A., Santos, J.F., Medina, J.M., Homam, S.M., 2011a. Sr-Nd isotope geochemistry and petrogenesis of the Chah-Shaljami granitoids (Lut Block, Eastern Iran). J. Asian Earth Sci. 41 (3), 283–296. https://doi.org/10.1016/j.jseaes.2011.02.014.
Arjmandzadeh, R., Karimpour, M.H., Mazaheri, S.A., Santos, J.F., Medina, J.M., Homam, S.M., 2011b. Two-sided asymmetric subduction; implications for tectonomagmatic and metallogenic evolution of the Lut Block, eastern Iran. J. Econ. Geol. 3 (1), P17–P30.
Asadi, S., Moore, F., Zarasvandi, A., 2014. Discriminating productive and barren porphyry copper deposits in the southeastern part of the central Iranian volcano-plutonic belt, Kerman region, Iran: a review. Earth-Sci. Rev. https://doi.org/10.1016/j.earscirev.2014.08.001.
Ayati, F., Yavuz, F., Asadi, H.H., Richards, J.P., Jourdan, F., 2013. Petrology and geochemistry of calc-alkaline volcanic and subvolcanic rocks, Dalli porphyry copper-gold deposit, Markazi Province, Iran. Int. Geol. Rev. 55 (2), 158–184. https://doi.org/10.1080/00206814.2012.689640.
Azizi, H., Tanaka, T., Asahara, Y., Chung, S.-L., Zarrinkoub, M.H., 2011. Discrimination of the age and tectonic setting for magmatic rocks along the Zagros thrust zone, northwest Iran, using the zircon U-Pb age and Sr–Nd isotopes. J. Geodyn. 52, 304–320.
Bach, W., Garrido, C.J., Paulick, H., Harvey, J., Rosner, M., 2004. Seawater-peridotite interactions: first insights from ODP Leg 209, MAR 15°N. Geochem., Geophys., Geosyst. 5 (9). https://doi.org/10.1029/2004GC000744.
Ballard, J.R., Palin, M.J., Campbell, I.H., 2002. Relative oxidation states of magmas inferred from Ce (IV)/Ce (III) in zircon: application to porphyry copper deposits of northern Chile. Contrib. Miner. Petrol. 144, 347–364. https://doi.org/10.1007/s00410-002-0402-5.
Bonatti, E., Lawrence, J.R., Morandi, N., 1984. Serpentinization of oceanic peridotites: temperature dependence of mineralogy and boron content. Earth Planet. Sci. Lett. 70 (1), 88–94.
Boschi, C., Früh-Green, G.L., Delacour, A., Karson, J.A., Kelley, D.S., 2006. Mass transfer and fluid flow during detachment faulting and development of an oceanic core complex, Atlantis Massif (MAR 30°N). Geochem. Geophys. Geosyst. 7 (1). https://doi.org/10.1029/2005GC001074.
Boynton, W.V., 1984. Geochemistry of the rare earth elements, Meteorite studies. In: Henderson, P. (Ed.), Rare Earth Element Geochemistry. Elsevier, Amsterdam, pp. 63–114.
Bromiley, G.D., Pawley, A.R., 2003. The stability of antigorite in the systems MgO-SiO2-H2O (MSH) and MgO-Al2O3-SiO2-H2O (MASH): the effects of Al3 + substitution on high-pressure stability. Am. Mineral. 88 (1), 99–108. https://doi.org/10.2138/am-2003-0113.
Candela, P.A., 1992. Controls on ore metal ratios in granite-related ore systems an experimental and computational approach. Trans. R. Soc. Edinb. Earth Sci. 83, 317–326. https://doi.org/10.1017/S0263593300007999.
César R. Ranero, Antonio Villaseñor, Jason Phipps Morgan, Wilhelm Weinrebe. Relationship between bend-faulting at trenches and intermediate-depth seismicity. Geochem., Geophys., Geosyst. 6(12), First published: 13 December 2005. Q12002, doi: 10.1029/2005GC000997.
Chiu, H.Y., Chung, S.L., Zarrinkoub, M.H., Mohammadi, S.S., 2013. Zircon U-Pb age constraints from Iran on the magmatic evolution related to Neo-Tethyan subduction and Zagros orogeny. Lithos 162–163, 70–87. https://doi.org/10.1016/j.lithos.2013.01.006.
Cao, M.J., Li, G.M., Qin, K.Z., Evans, N.J., Seitmuratova, E.Y., 2016. Assessing the magmatic affinity and petrogenesis of granitoids at the giant Aktogai porphyry Cu deposit, Central Kazakhstan. Am. J. Sci. 316, 614–668. https://doi.org/10.2475/07.2016.02.
Cao, M.J., Qin, K.Z., Li, G.M., Evans, N.J., Hollings, P., Maisch, M., Kappler, A., 2017. Mineralogical evidence for crystallization conditions and petrogenesis of ilmenite-series I-type granitoids at the Baogutu reduced porphyry Cu deposit (Western Junggar, NW China): Mössbauer spectroscopy, EPM and LA-(MC)-ICPMS analyses. Ore Geol. Rev. 86, 382–403. https://doi.org/10.1016/j.oregeorev.2017.02.033.
Cooke, D.R., Hollings, P., Walshe, J.L., 2005. Giant porphyry deposits: characteristics, distribution, and tectonic controls. Econ. Geol. 100 (5), 801–818. https://doi.org/10.2113/gsecongeo.100.5.801.
Defant, M.J., Drummond, M.S., 1993. Mount St. Helens: potential example of the partial melting of the subducted lithosphere in a volcanic arc. Geology 21 (6), 547–550.
Delacour, A., Früh-Green, G.L., Bernasconi, S.M., Schaeffer, P., Kelley, D.S., 2008. Carbon geochemistry of serpentinites in the Lost City Hydrothermal System (30°N, MAR). Geochim. Cosmochim. Acta 72 (15), 3681–3702. https://doi.org/10.1016/j.gca.2008.04.039.
Deng, C., Wan, Bo, Dong, Leilei, Talebian, Morteza, Windley, Brian F., Dadashzadeh, Hooman, Mohammadi, Behzad, Barati, Behzad, 2018. Miocene porphyry copper deposits in the Eastern Tethyan orogenic belt Using Sr- O isotopes and Sr/Y ratios to predict the source of ore related and Ore barren magmas. Gondwana Res. 62, 14–25. https://doi.org/10.1016/j.gr.2018.03.007.
Deschamps, F., Guillot, S., Godard, M., Andreani, M., Hattori, K., 2011. Serpentinites act as sponges for fluid-mobile elements in abyssal and subduction zone environments. Terra Nova 23, 171–178.
Deschamps, F., Godard, M., Guillot, S., Hattori, K., 2013. Geochemistry of subduction zone serpentinites: a review. Lithos. https://doi.org/10.1016/j.lithos.2013.05.019.
Dewey, J.F., Pitman, W.C., Ryan, W.B., Bonnin, J., 1973. Plate tectonics and the evolution of the Alpine system. Geol. Soc. Am. Bull. 84, 3137–3180.
Fakhari, M.D., Axen, G.J., Horton, B.K., Hassanzadeh, J., Amini, A., 2008. Revised age of proximal deposits in the Zagros foreland basin and implications for Cenozoic evolution of the High Zagros. Tectonophysics 451, 170–185. https://doi.org/10.1016/j.tecto.2007.11.064.
Ghiasvand, A., Karimpour, M.H., Malekzadeh Shafaroudi, A., Hidarian Shahri, M.R., 2018. Age and origin of subvolcanic rocks from NE Iran: Link between magmatic "flare-up" and mineralization. Chem. Erde 78, 254–267. https://doi.org/10.1016/j.chemer.2017.12.002.
Ghourchi, M., Karimpour, M.H., Farmer, G.L., Stern, C., 2014. Geology, alteration, age dating and petrogenesis of intrusive bodies in Halak Abad prospect area, NE Iran. J. Econ. Geol. 6 (1), 23–48.
Golestani, M., Karimpour, M.H., Malekzadeh Shafaroudi, A., Hidarian Shahri, M.R., 2018. Geochemistry, U-Pb geochronology and Sr-Nd isotopes of the Neogene igneous rocks, at the Iju porphyry copper deposit, NW Shahr-e-Babak, Iran. Ore Geol. Rev. 93, 290–307. https://doi.org/10.1016/j.oregeorev.2018.01.001.
Green, D.H., 1973. Experimental melting studies on a model upper mantle composition at high pressure under water-saturated and water-undersaturated conditions. Earth Planet. Sci. Lett. 19 (1), 37–53. https://doi.org/10.1016/0012-821X(73)90176-3.
Grove, T.L., Till, C.B., Lev, E., Chatterjee, N., Médard, E., 2009. Kinematic variables and water transport control the formation and location of arc volcanoes. Nature 459 (7247), 694–697. https://doi.org/10.1038/nature08044.
Grove, T.L., Till, C.B., Krawczynski, M.J., 2012. The role of H2O in Subduction Zone Magmatism. Annu. Rev. Earth Planet. Sci. 40, 413–439. https://doi.org/10.1146/annurev-earth-042711-105310.
Hacker, B.R., 2008. H2O subduction beyond arcs. Geochem., Geophys., Geosyst. 9 (3). https://doi.org/10.1029/2007GC001707.
Han, Y., Zhang, S., Pirajno, F., Zhou, X., Zhao, G., Qü, W., 2013. U-Pb and Re–Os isotopic systematics and zircon Ce4 + /Ce3 + ratios in the Shiyaogou Mo deposit in eastern Qinling, central China: insights into the oxidation state of granitoids and Mo (Au) mineralization. Ore Geol. Rev. 55, 29–47. https://doi.org/10.1016/j.oregeorev.2013.04.006.
Honarmand, M., Rashidnejad Omran, N., Carfu, F., Emami, M.H., Nabatian, G., 2013. Geochronology and magmatic history of a calc-alkaline plutonic complex in the Urumieh-Dokhtar Magmatic Belt, Central Iran: zircon ages as evidence for two major plutonic episodes. Abhandlungen, Neues Jahrbuch für Mineralogie 190 (1), 67–77. https://doi.org/10.1127/0077-7757/2013/0230.
Hossieni, R., Karimpour, M.H., Malekzadeh Shafaroudi, A., 2018. Petrography, geochemistry, U-Pb dating and Sr-Nd isotopes of igneous rocks in Tannurjeh porphyry Au-Cu prospect area (NE Kashmar). Petrology, 9th Year, No. 33, pp. 45–70.
Honarmand, M., 2016. Application of airborne geophysical and ASTER data for hydrothermal alteration mapping in the Sar-Kuh Porphyry Copper Area, Kerman Province. Iran. Open J. Geol. 6, 1257–1268. https://doi.org/10.4236/ojg.2016.610092.
Hou, Z.Q., Zhang, H., Pan, X., Yang, Z., 2011. Porphyry Cu (–Mo–Au) deposits related to melting of thickened mafic lower crust: examples from the eastern Tethyan metallogenic domain. Ore Geol. Rev. 39, 21–45.
Javidi Moghadam, M., Karimpour, M.H., Ebrahimi Nasrabadi, Kh, Hidarian Shahri, M.R., Malekzadeh, Shafaroudi A., 2018. Mineralogy, geochemistry, fluid inclusion and oxygen isotope investigations of epithermal Cu ± Ag veins of the Khur Area, Lut Block, Eastern Iran. Acta Geol. Sin. 92 (3), 1139–1156. https://doi.org/10.1111/1755-6724.13596.
Jarrard, R.D., 2003. Subduction fluxes of water, carbon dioxide, chlorine, and potassium. Geochem., Geophys., Geosyst. 4 (5). https://doi.org/10.1029/2002GC000392.
Karimpour, M.H., Malekzadeh Shafaroudi, A., Lang Farmer, G., Stern, C.R., 2012. U-Pb zircon geochronology, Sr-Nd isotopic characteristics, and important occurrence of Tertiary mineralization within the Lut block, eastern Iran. J. Econ. Geol. 4 (1). https://doi.org/10.22067/econg.v4i1.13391. Spring & Summer 2012, Serial No. 6.
Karimpour, M.H., Mazhari, N., Shafaroudi, A.M., 2014. Discrimination of different erosion levels of porphyry Cu deposits using ASTER image processing in eastern Iran: a case study in the Maherabad, Shadan, and Chah Shaljami areas. Acta Geol. Sin. 88 (4), 1195–1213. https://doi.org/10.1111/1755-6724.12283.
Karimpour, M.H., Sadeghi, M., 2018. Dehydration of hot oceanic slab at depth 30–50 km: KEY to formation of Irankuh-Emarat Pb-Zn MVT belt, Central Iran. J. Geochem. Explor. 194, 88–103. https://doi.org/10.1016/j.gexplo.2018.07.016.
Kazemi, K., Kananian, A., Xiao, Y., Sarjoughian, F., 2018. Petrogenesis of Middle-Eocene granitoids and their Mafic microgranular enclaves in central Urmia-Dokhtar Magmatic Arc (Iran): evidence for interaction between felsic and mafic magmas. Geosci. Front. 1–19. https://doi.org/10.1016/j.gsf.2018.04.006.
Kesler, S.E., Wilkinson, B.H., 2006. The role of exhumation in the temporal distribution of ore deposits. Econ. Geol. 101 (5), 919–922. https://doi.org/10.2113/gsecongeo.101.5.919.
Kesler, S.E., Chryssoulis, S.L., Simon, G., 2002. Gold in porphyry copper deposits: its

abundance and fate. Ore Geol. Rev. 21 (1–2), 103–124. https://doi.org/10.1016/S0169-1368(02)00084-7.
Kodolányi, J., Pettke, T., 2011. Loss of trace elements from serpentinites during fluid-assisted transformation of chrysotile to antigorite – an example from Guatemala. Chem. Geol. 284 (3–4), 351–362. https://doi.org/10.1016/j.chemgeo.2011.03.016.
Komeili, S.S., Khalili, M., Asadi Haroni, H., Bagheri, H., Ayati, F., 2017. The nature of hydrothermal fluids in the Kahang porphyry copper deposit (Northeast of Isfahan) based on mineralography, fluid inclusion and stable isotopic data. J. Econ. Geol. 8 (2), 285–305. https://doi.org/10.22067/econg.v8i2.37178. Autumn & Winter 2016-2017, Serial NO. 15.
Kushiro, I., 1974. Melting of hydrous upper mantle and possible generation of andesitic magma: an approach from synthetic systems. Earth Planet. Sci. Lett. 22 (4), 294–299. https://doi.org/10.1016/0012-821X(74)90138-1.
Lafay, R., Deschamps, F., Schwartz, S., Guillot, S., Godard, M., Debret, B., Nicollet, C., 2013. High-pressure serpentinites, a trap-and-release system controlled by metamorphic conditions: example from the Piedmont zone of the western Alps. Chem. Geol. 343, 38–54. https://doi.org/10.1016/j.chemgeo.2013.02.008.
Lee, C.T.A., Luffi, P., Chin, E.J., Bouchet, R., Dasgupta, R., Morton, D.M., Jin, D., 2012. Copper systematics in arc magmas and implications for crust-mantle differentiation. Science 335 (6077), 64–66. https://doi.org/10.1126/science.1217313.
Li, J.X., Qin, K.Z., Li, G.M., Cao, M.J., Xiao, B., Chen, L., Zhao, J.X., Evans, N.J., McInnes, B.I.A., 2012. Petrogenesis and thermal history of the Yulong porphyry copper deposit, Eastern Tibet: insights from U-Pb and U-Th/He dating, and zircon Hf isotope and trace element analysis. Mineral. Petrol. 105, 201–221.
Liang, H.Y., Campbell, I.H., Allen, C., Sun, W.D., Liu, C.Q., Yu, H.X., 2006. Zircon Ce4+/Ce3+ ratios and ages for Yulong ore-bearing porphyries in eastern Tibet. Miner. Deposita 41, 152–159.
Magni, V., Faccenna, C., van Hunen, J., Funiciello, F., 2014. How collision triggers backarc extension: insight into Mediterranean style of extension from 3-d numerical models. Geology 42 (6), 511–514. https://doi.org/10.1130/G35446.1.
Mahdavi, A., Karimpour, M.H., Mao, J., Haidarian Shahri, M.R., Malekzadeh Shafaroudi, A., Li, H., 2016. Zircon U-Pb geochronology, Hf isotopes and geochemistry of intrusive rocks in the Gazu copper deposit, Iran: petrogenesis and geological implications. Ore Geol. Rev. 72, 818–837. https://doi.org/10.1016/j.oregeorev.2015.09.011.
Malekzadeh Shafaroudi, A., Karimpour, M.H., Mazaheri, S.A., 2010. Rb–Sr and Sm–Nd isotopic compositions and Petrogenesis of ore-related intrusive rocks of gold-rich porphyry copper Maherabad prospect area (north of Hanich), east of Iran. J. Crystallogr. Mineral 18 (2), 15–32 Summer 1389/2010.
Malekzadeh Shafaroudi, A., Karimpour, M.H., Stern, C.R., 2015. The Khopik porphyry copper prospect, Lut Block, Eastern Iran: geology, alteration and mineralization, fluid inclusion, and oxygen isotope studies. Ore Geol. Rev. 65 (P2), 522–544. https://doi.org/10.1016/j.oregeorev.2014.04.015.
McInnes, B.I.A., Evans, N.J., Belousova, E., Griffin, W.T., Andrew, R.L., 2003. Timing of mineralization and exhumation processes at the Sarcheshmeh and Meiduk porphyry Cu deposits, Kerman belt, Iran. In: Eliopoulos (Ed.), Mineral Exploration and Sustainable Development (7th Biennial SGA Meeting, Athens, August 24–28). Millpress, Rotterdam, pp. 1197–1200.
McInnes, B.I.A., Evans, N.J., Fu, F.Q., Garwin, S., Belousova, E., Griffin, W.L., Bertens, A., Sukama, D., Permanadewi, S., Andrew, R.L., Deckart, K., 2005. Thermal history analysis of selected Chilean, Indonesian, and Iranian porphyry Cu–Mo–Au deposits. In: Porter, T.M. (Ed.), Super Porphyry Copper and Gold Deposits: A Global Perspective. PGC publishing, Adelaide, pp. 1–16.
Mineral Commodity Summaries, 2018. U.S. Department of the Interior, U.S. Geological Survey.
Miri Beydokhti, R.M., Karimpour, M.H., Mazaheri, S.A., Santos, J.F., Klötzli, U., 2015. U-Pb zircon geochronology, Sr-Nd geochemistry, petrogenesis and tectonic setting of Mahoor granitoid rocks (Lut Block, Eastern Iran). J. Asian Earth Sci. 111, 192–205. https://doi.org/10.1016/j.jseaes.2015.07.028.
Mirnejad, H., Mathur, R., Hassanzadeh, J., Shafie, B., Nourali, S., 2013. Linking cu mineralization to host porphyry emplacement: Re-Os ages of molybdenites versus U-Pb ages of zircons and sulfur isotope compositions of pyrite and chalcopyrite from the IJU and Sarkuh porphyry deposits in southeast Iran. Econ. Geol. 108 (4), 861–870. https://doi.org/10.2113/econgeo.108.4.861.
Moradi Noghondar, M., Karimpour, Mohammad Hassan, Shafaroudi, Azadeh Malekzadeh, Lang Farmer, G., Stern, Charles, 2012. Geochemistry, zircon U-Pb geochronology and Rb-Sr & Sm-Nd isotopes of Najmabad monzonitic rocks south of Ghonabad. Petrology 76–95 3rd Year, No. 11.
Mouthereau, F., Lacombe, O., Verges, J., 2012. Building the Zagros collisional orogen: timing, strain distribution and the dynamics of Arabia/Eurasia plate conver-gence. Tectonophysics 532, 27–60. https://doi:10.1016/j.tecto.2012.01.022.
Mungall, J.E., 2002. Roasting the mantle: slab melting and the genesis of major Au and Au-rich Cu deposits. Geology 30 (10), 915–918. https://doi.org/10.1130/0091-7613(2002) 030<0915:RTMSMA>2.0.CO;2.
Novella, D., Dolejš, David, Myhill, Robert, Pamato, Martha G., Manthilake, Geeth, Frost, Daniel J., 2017. Melting phase relations in the systems Mg2SiO4–H2O and MgSiO3–H2O and the formation of hydrous melts in the upper mantle. Geochim. Cosmochim. Acta 204, 68–82. https://doi.org/10.1016/j.gca.2016.12.042.
Omrani, J., Agard, P., Whitechurch, H., Benoit, M., Prouteau, G., Jolivet, L., 2008. Arc-magmatism and subduction history beneath the Zagros Mountains, Iran: a new report of adakites and geodynamic consequences. Lithos 106, 380–398. https://doi.org/10.1016/j.lithos.2008.09.008.
Peacock, S.M., Wang, K., 1999. Seismic consequences of warm versus cool subduction metamorphism: examples from southwest and northeast Japan. Science 286 (5441), 937–939. https://doi.org/10.1126/science.286.5441.937.
Pearce, J.A., Harris, N.B.W., Tindle, A.G., 1984. Trace element discrimination diagrams for the tectonic interpretation of granitic rocks. J. Petrol. 25 (4), 956–983. https://doi.org/10.1093/petrology/25.4.956.
Perrillat, J.P., Daniel, I., Koga, K.T., Reynard, B., Cardon, H., Crichton, W.A., 2005. Kinetics of antigorite dehydration: a real-time X-ray diffraction study. Earth Planet. Sci. Lett. 236 (3–4), 899–913. https://doi.org/10.1016/j.epsl.2005.06.006.
Pirajno, F., 2009. Hydrothermal processes and mineral systems. Hydrotherm. Process. Mineral Syst. https://doi.org/10.1007/978-1-4020-8613-7.
Pirouz, M., Avouac, Jean-Philippe, Hassanzadeh, Jamshid, Kirschvink, Joseph L., Bahroudi, Abbas, 2017. Early Neogene foreland of the Zagros, implications for the initial closure of the Neo-Tethys and kinematics of crustal shortening. Earth Planet. Sci. Lett. 477, 168–182. https://doi.org/10.1016/j.epsl.2017.07.046.
Razique, A., Lo Grasso, G., Livesey, T., 2007. Porphyry Copper–Gold Deposits at Reko Diq Complex, Chagai Hills Pakistan. Proceedings of Ninth Biennial SGA Meeting, Dublin.
Richards, J., 2011. High Sr/Y arc magmas and porphyry Cu ± Mo ± Au deposits: Just add water. Econ. Geol. 106 (7), 1075–1081. https://doi.org/10.2113/econgeo.106.7.1075.
Richards, J.P., 2003. Tectono-magmatic precursors for porphyry Cu-(Mo-Au) deposit formation. Econ. Geol. 98 (8), 1515–1533. https://doi.org/10.2113/gsecongeo.98.8.1515.
Richards, J.P., Spell, T., Rameh, E., Razique, A., Fletcher, T., 2012. High Sr/Y magmas reflect arc maturity, high magmatic water content, and porphyry Cu ± Mo ± Au potential: examples from the Tethyan arcs of central and eastern Iran and Western Pakistan. Econ. Geol. 107 (2), 295–332. https://doi.org/10.2113/econgeo.107.2.295.
Richards, J.P., 2015. Tectonic, magmatic, and metallogenic evolution of the Tethyan orogen: from subduction to collision. Ore Geol. Rev. 70, 323–345. https://doi.org/10.1016/j.oregeorev.2014.11.009.
Richards, J.P., 2018. Why is my porphyry a dud? RFG 2018 Conference Proceeding, June 16–21, 2018. Vancouver, Canada.
Rowan, L.C., Hook, S.J., Abrams, M.J., Mars, J.C., 2003. Mapping hydrothermally altered rocks at Cuprite, Nevada, using the Advanced Spaceborne Thermal Emission and Reflection Radiometer (ASTER), A new satellite- imaging system. Econ. Geo. 98 (5), 1019–1027. https://doi.0361-0128/01/3366/1019-9.
Rudnick, R.L., Fountain, D.M., 1995. Nature and composition of the continental crust: a lower crustal perspective. Rev. Geophys. https://doi.org/10.1029/95RG01302.
Rüpke, L.H., Morgan, J.P., Hort, M., Connolly, J.A.D., 2004. Serpentine and the subduction zone water cycle. Earth Planet. Sci. Lett. 223 (1–2), 17–34. https://doi.org/10.1016/j.epsl.2004.04.018.
Scambelluri, M., Müntener, O., Ottolini, L., Pettke, T.T., Vannucci, R., 2004. The fate of B, Cl and Li in the subducted oceanic mantle and in the antigorite breakdown fluids. Earth Planet. Sci. Lett. 222 (1), 217–234. https://doi.org/10.1016/j.epsl.2004.02.012.
Seedorff, E., Dilles, John H., Proffett Jr., John M., Einaudi, Marco T., Zurcher, Lukas, Stavast, William J.A., Johnson, David A., Barton, Mark D., 2005. Porphyry deposits: Characteristics and origin of hypogene features. Econ. Geol. 100th, Anniversary Volume, 251–298. https://doi.org/10.5382/AV100.10.
Shafiei, B., 2010. Lead isotope signatures of the igneous rocks and porphyry copper deposits from the Kerman Cenozoic magmatic arc (SE Iran), and their magmatic– metallogenetic implications. Ore Geol. Rev. 38, 27–36. https://doi.org/10.1016/j.oregeorev.2010.05.004.
Shafiei, B., Shahabpour, J., 2008. Gold distribution in porphyry copper deposits of Kerman Region, South-eastern Iran. J. Sci., Islamic Republic of Iran 19 (3), 247–260 University of Tehran, ISSN 1016-1104 247.
Shafiei, B., Haschke, M., Shahabpour, J., 2009a. Recycling of orogenic arc crust triggers porphyry Cu mineralization in Kerman Cenozoic arc rocks, southeastern Iran. Miner. Deposita. 44, 265–283.
Shafiei, B., Shahabpour, J., Haschke, M., 2008. Transition from Paleogene normal calcalkaline to neogene adakitic-like plutonism and Cu-metallogeny in the Kerman porphyry copper belt: response to neogene crustal thickening. J. Sci. Islam. 19, 67–84.
Sarjoughian, F., Kananian, A., 2017. Zircon U-Pb geochronology and emplacement history of intrusive rocks in the Ardestan section, central Iran. Geologica Acta 15 (1), 25–36. https://doi.org/10.1344/GeologicaActa 2017.15.1.3. I-X.
Shafiei, B., Haschke, M., Shahabpour, J., 2009b. Recycling of orogenic arc crust triggers porphyry Cu mineralization in Kerman Cenozoic arc rocks, southeastern Iran. Miner. Deposita 44 (3), 265–283. https://doi.org/10.1007/s00126-008-0216-0.
Shahabpour, J., Kramers, J.D., 1987. Lead isotope data from the Sar-Cheshmeh porphyry copper deposit. Miner. Deposita. 22, 278–281.
Shen, P., Hattori, K., Pan, H., Jackson, S., Seitmuratova, E., 2015. Oxidation condition and metal fertility of granitic magmas: zircon trace-element data from porphyry cu deposits in the central Asian orogenic belt. Econ. Geol. 110 (7), 1861–1878. https://doi.org/10.2113/econgeo.110.7.1861.
Sillitoe, R.H., 2010. Porphyry copper systems. Econ. Geol. 105 (1), 3–41. https://doi.org/10.2113/gsecongeo.105.1.3.
Simon, A.C., Pettke, T., Candela, P.A., Piccoli, P.M., Heinrich, C.A., 2006. Copper partitioning in a melt-vapor-brine-magnetite-pyrrhotite assemblage. Geochim. Cosmochim. Acta 70 (22), 5583–5600. https://doi.org/10.1016/j.gca.2006.08.045.
Simon, A.C., Candela, P.A., Piccoli, P.M., Mengason, M., Englander, L., 2008. The effect of crystal-melt partitioning on the budgets of Cu, Au, and Ag. Am. Mineral. 93 (8–9), 1437–1448. https://doi.org/10.2138/am.2008.2812.
Singer, D.A., Berger, V.I., Moring, B.C., 2008. Porphyry copper deposits of the world: database and grade and tonnage. U.S. Geological Survey Open-File Report 2008–1155.
Smythe, D.J., Brenan, J.M., 2015. Cerium oxidation state in silicate melts: combined fO2, temperature and compositional effects. Geochim. Cosmochim. Acta 170, 173–187. https://doi.org/10.1016/j.gca.2015.07.016.

Smythe, D.J., Brenan, J.M., 2016. Magmatic oxygen fugacity estimated using zircon-melt partitioning of cerium. Earth Planet. Sci. Lett. 453, 260–266. https://doi.org/10.1016/j.epsl.2016.08.013.

Sun, W., Huang, R.F., Li, H., Hu, Y.B., Zhang, C.C., Sun, S.J., et al., 2015. Porphyry deposits and oxidized magmas. Ore Geol. Rev. https://doi.org/10.1016/j.oregeorev.2014.09.004.

Sun, W.D., Liang, H.Y., Ling, M.X., Zhan, M.Z., Ding, X., Zhang, H., Fan, W.M., 2013. The link between reduced porphyry copper deposits and oxidized magmas. Geochim. Cosmochim. Acta 103, 263–275. https://doi.org/10.1016/j.gca.2012.10.054.

Sun, W.D., Huang, R.F., Liang, H.Y., Ling, M.X., Li, C.Y., Ding, X., Zhang, H., Yang, X.Y., Ireland, T., Fan, W.M., 2014a. Magnetite–hematite, oxygen fugacity, adakite and porphyry copper deposits: reply to Richards. Geochim. Cosmochim. Acta 126, 646–649.

Sun, W.D., Zhanf, C.C., Liang, H.Y., Ling, M.X., Li, C.Y., Ding, X., Zhang, H., Yang, X.Y., 2014b. The genetic association between magnetite–hematite and porphyry copper deposits: reply to Pokrovski. Geochim. Cosmochim. Acta 126, 639–642 (Takagi, T., 2004. Origin of magnetite- and ilmenite-series granitic rocks in the Japan Arc. Am. J. Sci. 304 (2), 169–202. https://DOI: 10.1016/j.gca.2013.07.038).

Sun, W., Wang, J.-T., Zhang, L.-P., Zhang, C.-C., Li, H., Ling, M.-X., Ding, X., Li, C.-Y., Liang, H.-Y., 2016. The formation of porphyry copper deposits. Acta Geochim. 36 (1), 9–15. https://doi.org/10.1007/s11631-016-0132-4.

Syracuse, E.M., Abers, G.A., 2006. Global compilation of variations in slab depth beneath arc volcanoes and implications. Geochem., Geophys., Geosyst. 7 (5). https://doi.org/10.1029/2005GC001045.

Syracuse, E.M., van Keken, P.E., Abers, G.A., Suetsugu, D., Bina, C., Inoue, T., Jellinek, M., 2010. The global range of subduction zone thermal models. Phys. Earth Planet. Inter. 183 (1–2), 73–90. https://doi.org/10.1016/j.pepi.2010.02.004.

Taghipour, N., 2007. The application of fluid inclusions and isotope geochemistry as guides for exploration, alteration and mineralization at the Meiduk porphyry copper deposit, Shahr-Babak, Kerman. Unpublished Ph.D. thesis, Shaheed Bahonar University, Kerman, Iran, p. 321.

Taghipour, N., Aftabi, A., Mathur, R., 2008. Geology and Re–Os geochronology of mineralization of the Miduk porphyry copper deposit. Resour. Geol. 2, 143–160.

Trail, D., Bruce Watson, E., Tailby, N.D., 2012. Ce and Eu anomalies in zircon as proxies for the oxidation state of magmas. Geochim. Cosmochim. Acta 97, 70–87. https://doi.org/10.1016/j.gca.2012.08.032.

Ulmer, P., Trommsdorff, V., 1995. Serpentine stability to mantle depths and subduction-related magmatism. Science 268 (5212), 858–861. https://doi.org/10.1126/science.268.5212.858.

USGS, 2010. Mineral Resources On-Line Spatial Data. < https://mrdata.usgs.gov/sir20105090z/show-sir20105090z.php?id=9224 > .

Van Keken, P.E., Hacker, B.R., Syracuse, E.M., Abers, G.A., 2011. Subduction factory: 4. Depth-dependent flux of H2O from subducting slabs worldwide. J. Geophys. Res.: Solid Earth 116 (1). https://doi.org/10.1029/2010JB007922.

Vils, F., Müntener, O., Kalt, A., Ludwig, T., 2011. Implications of the serpentine phase transition on the behaviour of beryllium and lithium-boron of subducted ultramafic rocks. Geochim. Cosmochim. Acta 75 (5), 1249–1271. https://doi.org/10.1016/j.gca.2010.12.007.

Wada, I., Wang, K., 2009. Common depth of slab-mantle decoupling: reconciling diversity and uniformity of subduction zones. Geochem. Geophys. Geosyst. 10 (10). https://doi.org/10.1029/2009GC002570.

Wan, B., Deng, C., Najafi, A., Hezareh, M.R., Talebian, M., Dong, L., Xiao, W., 2018. Fertilizing porphyry Cu deposits through deep crustal hot zone melting. Gondwana Res. 60, 179–185. https://doi.org/10.1016/j.gr.2018.04.006.

Wang, R., Richards, J.P., Hou, Z.Q., Yang, Z.M., Gu, Z.B., DuFrane, S.A., 2014. Increasing magmatic oxidation state from Paleocene to Miocene in the eastern Gangdese Belt, Tibet: implication for collision-related porphyry Cu-Mo +/_ Au mineralization. Econ. Geol. 109, 1943–1965.

Wang, J., Zhao, D., Yao, Z., 2017. Seismic anisotropy evidence for dehydration embrittlement triggering intermediate-depth earthquakes. Sci. Rep. 7 (1). https://doi.org/10.1038/s41598-017-02563-w.

Wu, S., Zheng, Y.Y., Sun, X., 2016. Subduction metasomatism and collision-related metamorphic dehydration controls on the fertility of porphyry copper ore-forming high Sr/Y magma in Tibet. Ore Geol. Rev. 73, 83–103.

White, W.M., Klein, E.M., 2013. Composition of the Oceanic Crust. Treatise Geochem. Second Ed. 4, 457–496. https://doi.org/10.1016/B978-0-08-095975-7.00315-6.

Wilkinson, B.H., Kesler, S.E., 2009. Quantitative identification of metallogenic epochs and provinces: application to phanerozoic porphyry copper deposits. Econ. Geol. 104 (5), 607–622. https://doi.org/10.2113/gsecongeo.104.5.607.

Wunder, B., Schreyer, W., 1997. Antigorite: high-pressure stability in the system MgO-SiO2-H2O (MSH). Lithos 41 (1–3), 213–227. https://doi.org/10.1016/S0024-4937(97)82013-0.

Zarasvandi, A., Liaghat, S., Zentilli, M., 2005. Geology of the Darreh-Zerreshk and Ali-Abad porphyry copper deposits, Central Iran. Int. Geol. Rev. 47 (6), 620–646. https://doi.org/10.2747/0020-6814.47.6.620.

Zarasvandi, A., Rezaei, M., Sadeghi, M., Lentz, D., Adelpour, M., Pourkaseb, H., 2015. Rare earth element signatures of economic and sub-economic porphyry copper systems in Urumieh-Dokhtar Magmatic Arc (UDMA), Iran. Ore Geol. Rev. 70, 407–423. https://doi.org/10.1016/j.oregeorev.2015.01.010.

Zhang, H., Li, C.Y., Yang, X.Y., Sun, Y.L., Deng, J.H., Liang, H.Y., 2014. Shapinggou: the largest Climax-type porphyry Mo deposit in China. Int. Geol. Rev. 56, 313–331.

Zhang, C. Chan, Sun, W. Dong, Wang, J. Tuan, Zhang, L. Peng, Sun, S. Jun, Wu, K., 2017. Oxygen fugacity and porphyry mineralization: a zircon perspective of Dexing porphyry Cu deposit, China. Geochim. Cosmochim. Acta 206, 343–363. https://doi.org/10.1016/j.gca.2017.03.013.